CONFOCAL MICROSCOPY STUDIES OF COLLOIDAL ASSEMBLY ON MICROFABRICATED PHYSICALLY TEMPLATED SURFACES

A Thesis

by

SUMIT SHARMA

Submitted to the Office of Graduate Studies of
Texas A&M University
in partial fulfillment of the requirements for the degree of

MASTER OF SCIENCE

December 2004

Major Subject: Chemical Engineering

CONFOCAL MICROSCOPY STUDIES OF COLLOIDAL ASSEMBLY ON MICROFABRICATED PHYSICALLY TEMPLATED SURFACES

A Thesis

by

SUMIT SHARMA

Submitted to Texas A&M University
in partial fulfillment of the requirements
for the degree of

MASTER OF SCIENCE

Approved as to style and content by:

Michael A. Bevan (Chair of Committee)	Victor M. Ugaz (Member)
Kenneth R. Hall (Head of Department)	Terry Creasy (Member)

December 2004

Major Subject: Chemical Engineering

ABSTRACT

Confocal Microscopy Studies of Colloidal Assembly
on Microfabricated Physically Templated Surfaces. (December 2004)
Sumit Sharma, B.Tech., Jawaharlal Nehru Technological University
Chair of Advisory Committee: Dr. Michael A. Bevan

In this research we consider two different approaches for microfabricating physical templates to be used in template directed colloidal self-assembly experiments. Fabrication of templates, usable with confocal microscopy, forms an essential part of observation and analysis of template directed colloidal self-assembly studies. We use existing laboratory based microfabrication methods for patterning thin glass coverslips and polymeric films. These templates when used for directing colloidal self-assembly along with confocal microscopy analysis provide us with relevant information on the effect of confined geometries of the template on particle packing and order.

The first method of template fabrication involves ultraviolet photolithography, thin film deposition, and glass micro machining. Various stages of the process were optimized while selecting reactive ion etch (RIE) and nickel etch mask with a suitable etch recipe for microfabrication of patterns on thin multi-component glass coverslips. Pattern dimensions were shown to be nearly commensurate with patterns on the microfiche, which was used as a field mask. In another approach, mechanical machining for fabricating polymeric templates was attempted on poly(methyl methacrylate) films spin coated on thin glass cover slips. The mechanical machining was implemented using computer numerical control (CNC) machines with the pattern dimensions in the range of 50µm-150µm.

The glass and polymeric templates were used in template directed colloidal self-assembly experiments using polystyrene or silica particles. Confocal microscopy was used to obtain images of particle packing in template geometries. Imaging of the

particles confined in the template geometries show increased particle concentration along pattern walls and corners. Inherent pattern irregularities and roughness possibly resulted in limited order in particle. Using a simple fortran program, image stack generated from confocal microscopy is used for obtaining images of particle packing in four different view planes which includes top, side, cross sectional and diagonal view of the image stack.

The results from this research show the application of simple microfabrication processes for creating physical templates for template directed colloidal self-assembly. Confocal microscopy imaging combined with fortran image processing program can provide images of particle packing in different view planes. These images of the particles confined in various pattern geometries illustrate greater possibility of packing order in straight and regular pattern geometries or profiles.

To my parents and brother

ACKNOWLEDGMENTS

I would like to express my sincere gratitude to my advisor Dr. Michael A. Bevan for the guidance and independence given to me in this research. I am grateful to Dr. Terry Creasy for helping and guiding me with the CNC machining and providing me with the necessary machining facilities for my research. I would like to thank Dr. Victor M. Ugaz for the insightful discussions I was able to have with him related to my research. I also thank both Dr. Creasy and Dr. Ugaz for being on my advisory committee. I am thankful to Dr. William M. Lackowski, Yulia Vasilyeva and the material characterization facility for all the materials and equipment made available to me for my research work. I also thank Kim Jong Hyun for helping me learn CNC machining. I am also thankful to Samartha G. Anekal, Hung-Jen Wu, Pradipkumar Bahukudumbi, Richard Beckham and Gregory Fernandes for all the helpful discussions I was able to have with them regarding my research experiments. I am grateful to the department of chemical engineering for giving me the opportunity to pursue graduate studies here at Texas A&M.

I wish to thank each and everyone of the people who have directly or indirectly helped me in realizing my present research and educational goals.

TABLE OF CONTENTS

Page

ABSTRACT iii

DEDICATION v

ACKNOWLEDGMENTS vi

TABLE OF CONTENTS vii

LIST OF FIGURES x

LIST OF TABLES xiii

1. INTRODUCTION 1

- 1.1 Objectives and significance 1
- 1.2 Historical perspective 3
- 1.3 Recent literature review 3
  - 1.3.1 Applications of colloidal crystals 3
  - 1.3.2 Use of physical templates for colloidal deposition 4
  - 1.3.3 Glass micromachining 7
  - 1.3.4 Ultraprecision machining of polymers 8
- 1.4 Summary of conclusions 9

2. EXPERIMENTAL 11

- 2.1 Microfiche mask preparation 11
- 2.2 Glass substrate preparation 13
  - 2.2.1 Photolithography 15
  - 2.2.2 Wet etching 16
  - 2.2.3 Reactive ion etching 18
- 2.3 Mechanical machining 20
- 2.4 Confocal microscopy imagining experiments 21

3. PHOTOLITHOGRAPHY AND GLASS MICROMACHINING FOR PHYSICAL PATTERNING OF TEMPLATES 25

- 3.1 Introduction 25
- 3.2 Experimental 27
  - 3.2.1 Materials 27
  - 3.2.2 Substrate preparation procedure 27
  - 3.2.3 Etch rate and profile determination using confocal microscopy 29
- 3.3 Results and discussion 29
  - 3.3.1 Ultraviolet photolithography 29
  - 3.3.2 Wet etching 31
  - 3.3.3 Reactive ion etching 32

Page

3.4 Conclusions 50

4. PATTERNING OF TEMPLATES BY MECHANICAL MACHINING OF POLYMERIC FILMS 51

4.1 Introduction 51
4.2 Experimental 52
4.2.1 Materials 52
4.2.2 Substrate preparation procedure 53
4.2.3 PMMA machining 53
4.3 Results and discussion 54
4.3.1 Spin coating 54
4.3.2 Holes: Cut spin speed and z-speed 56
4.3.3 Number of repeats 61
4.3.4 Machining of lines 65
4.4 Conclusions 66

5. OBSERVATION OF PARTICLE PACKING ON TEMPLATE PATTERNS USING CONFOCAL MICROSCOPY 68

5.1 Introduction 68
5.2 Experimental 70
5.2.1 Materials 70
5.2.2 Substrate preparation procedure 70
5.2.3 Colloidal sample preparation 71
5.2.4 Confocal scanning laser microscopy 71
5.2.5 Fortran image processing 72
5.3 Results and discussion 74
5.3.1 Imaging of glass substrates 74
5.3.2 Imaging of PMMA substrates 79
5.4 Conclusions 83

6. CONCLUSIONS 84

6.1 Summary 84

7. FUTURE RESEARCH 87

7.1 Nanoindenting for patterning polymeric substrates 87
7.2 Electrophoretic deposition of colloids on patterned substrates 89
7.3 Quantitative assessment of template directed colloidal crystallization.. 90
7.4 Diffusing colloidal probe microscopy 91

Page
REFERENCES 92
VITA 98

LIST OF FIGURES

FIGURE Page

2.1 Pattern on microfiche 12

2.2 Steps in glass substrate patterning........ 14

2.3 Steps in ultraviolet photolithography 16

2.4 Schematic for reactive ion etching 19

2.5 Fortran image processing: View planes from Fortran imaging........ 24

3.1 Steps in ultraviolet photolithography pattern transfer........ 26

3.2 Pattern on photoresist after 25 seconds of uv exposure 30

3.3 Etch profile of coverslip etched in 1:20 BOE for 60 minutes........ 31

3.4 Etch profile of coverslip etched in 1:10 BOE for 60 minutes........ 31

3.5 Etch profile of coverslip etched in 1:5 BOE for 60 minutes........ 32

3.6 Reactive ion etching of corning 0211 with chrome etch mask, CF_4:O_2 at 14:2 flow rate and etched for 15 minutes at power P=200W........ 34

3.7 Annealed corning 0211 with chrome etch mask 35

3.8 Corning 0211 glass with chrome etch mask, etched in 100% CF_4 35

3.9 Etch profile of borofloat glass........ 35

3.10 Etch profile of corning 0211 glass with chrome etch mask and intermittent acid wash 36

3.11 Reactive ion etching of corning 0211 with aluminum etch mask........ 37

3.12 100% CF_4 and aluminum etch mask 37

3.13 Effect of gas flow ratio on etch profile: CF_4:O_2 at 14:2 flow rate ratio 38

3.14 Effect of gas flow ratio on etch profile: CF_4:O_2 at 8:8 flow rate ratio 38

3.15 Effect of gas flow ratio on etch profile: CF_4:O_2 at 4:12 flow rate ratio 39

3.16 Effect of gas flow ratio on etch profile: CF_4:O_2 at 2:14 flow rate ratio 39

FIGURE Page

3.17 Coverslip etched at an etch gas flow rate of 10 sccm with 3:7 ratio of $CF_4:O_2$ at 200W 41

3.18 Effect of power on etch rates: P=100W 41

3.19 Effect of power on etch rates: P=150W 42

3.20 Effect of power on etch rates: P=200W 42

3.21 Effect of power on etch rates: P=250W 43

3.22 Effect of power on etch rates: P=300W 43

3.23 Corning 0211 etch profile for 30 minutes RIE 45

3.24 Corning 0211 etch profile for 60 minutes RIE 45

3.25 Corning 0211 etch profile for 30 minutes RIE, 5 minutes intermittent HCl wash, nickel mask 46

3.26 Corning 0211 etch profile for 30 minutes RIE, 10 minutes intermittent HCl wash, nickel mask 46

3.27 Corning 0211 etch profile for 30 minutes RIE, 15 minutes intermittent HCl wash, nickel mask 47

3.28 Etch profile with chrome adhesive layer 48

3.29 Top view of the sample with chrome layer as adhesive metal for nickel mask 48

3.30 A 5nm chrome adhesive layer and nickel etch mask still resulted in trenching and metal mask erosion 49

3.31 Corning 0211 etch profile with intermittent 1M HCl wash after every 15 minutes for total 45 minutes of RIE 50

4.1 CNC machined hole on PMMA 58

4.2 Side view of the CNC machined hole 59

4.3 One time machined hole at a cut spin speed of 3000rpm 60

4.4 One time machined hole at a cut spin speed of 8000rpm 61

FIGURE Page

4.5 Hole machined repeatedly three times at 5300rpm 62
4.6 Hole machined at a speed of 8000rpm repeatedly three times....................... 63
4.7 Cutting tool machined the PMMA to the glass surface: Side view 63
4.8 Cutting tool machined the PMMA to the glass surface: Layered top views.... 64
4.9 Line machined at a tool speed of 8000rpm 65
4.10 Wake of tool (right) while machining line on PMMA.................................. 66
5.1 Fortran imaging: View planes 73
5.2 Colloids in channels patterned using glass wet etching 75
5.3 Colloids in curvilinear channels 77
5.4 Colloids in pseudo rectangular channels patterned using reactive ion etching 78
5.5 View planes of colloids in pseudo rectangular channels................................ 79
5.6 Silica particles confined in the rough geometries of the PMMA substrate...... 80
5.7 6µm colloidal particles arranged in the machined PMMA hole 81
5.8 Polystyrene particles in the patterned hole with glass bottom and PMMA side walls 82
7.1 A nanoindentor basic set up 87
7.2 Simple hole pattern made using nanoindentor on a polymeric film 88
7.3 Electrophoretic deposition set up with ITO coated on patterned coverslips.... 90

LIST OF TABLES

TABLE Page

2.1 Types of glasses used in experiments 13
2.2 Etch masks description 15
3.1 Metal etch masks description 28
3.2 Wet etching: Summary 32
3.3 Dry etching with chrome etch mask 35
3.4 Dry etching with aluminum etch mask 37
3.5 Etch gas flow ratios and glass etch rates 40
3.6 Effect of power on etch rates 44
3.7 Effect of duration of etch 45
3.8 Effect of intermittent HCl wash on corning 0211 glass etch rate and profile 47
3.9 Effect of chrome adhesive layer 50
4.1 Summary of PMMA spin coating 56

1. INTRODUCTION

1.1 Objectives and significance

The objective of this research work is to fabricate physical templates for template directed colloidal self-assembly, using photolithography and mechanical machining methods. Ease of pattern fabrication and reproducibility are the two important considerations, which have guided this research. Both polymeric and non-polymeric substrates can be used to guide colloidal self-assembly and therefore their fabrication process becomes an essential part of the study. The physical templates in this research conform to the confocal microscopy analysis requirements. In the later part of this research, confocal microscopy is used for observing the packing of colloids in the confined features of the template geometries.

The fabrication of physical templates using photolithography and mechanical methods considered in this research could ensure a simple and easy way of patterning substrates using the available laboratory methods. Of the two approaches used in this research, the first approach applies the general ultraviolet photolithography techniques in the initial stages of the pattern transfer process on to the glass substrates, using a microfiche photomask. The multi-component glass coverslips were used as substrates and were patterned using wet and dry etching techniques. In order to avoid the undercut resulting from the wet etching of glass coverslips, dry etching method was preferred, which is a better method to obtain directional etching of the substrate. The method is also important as it gives the ability to gain some leverage on pattern dimensions by controlled etching.

This thesis follows the style of *Langmuir*.

Unlike quartz coverslips, for multi-component coverslips, which are more common and cost much less, the reactive ion etch method is not a straightforward method. In this research, an intermittent acid wash was attempted as a way to remove the non-SiO_2 contents which otherwise make the etch process difficult.

The second method involves ultrafine machining of poly(methyl methacrylate) (PMMA) film spin coated on glass cover slips. In this method computer aided numeric control machine (CNC) is used for microfabrication, which provides a novel way of patterning polymeric templates for colloidal deposition. Computerized process provides enhanced control on both pattern design and fabrication. The speed and depth of cut is controlled using the machining program, which also directs the cutting tool precisely along the specified positions and patterns to be machined on the substrate. Using one of the smallest size tools available for CNC machining, potential energy wells, or holes approximately 10μm deep, were fabricated in terms of holes on the PMMA substrate.

The glass and polymeric templates, fabricated using the methods pursued, are thin as well as optically transparent so that they can be used for confocal microscopy analysis. In the final part of this research, the templates are used in colloidal deposition experiments. Particles are made to close pack in the confined features of the patterns under the influence of gravity and capillary forces arising from drying process. Confocal microscopy is used for observing the particle packing in these patterns. The particles, in a refractive index matched fluorescent medium, are seen to pack in the template geometries with limited order. The images of the particle packing in different view planes, generated by a combination confocal microscopy and a simple Fortran program, help in better and independent visualization of template directed colloidal self-assembly process. Effect of particle size and pattern dimensions on the particle packing is of particular interest due to its significance in colloidal crystallization and hence the photonic and numerous other applications.

1.2 Historical perspective

It was well known that monodisperse colloids, capable of forming long-range order structures existed in nature with the discovery of tobacco and tomato viruses by Stanley (1935).[1] The work by Sanders (1968)[2] and Iler (1979)[3] attributed the brilliant opalescence of opals to well ordered structure of silica colloids. The ability to form long-range order colloidal crystals was made possible at laboratory scale after the work by Stober (1968)[4] and Iler (1979)[3] on monodisperse colloidal particle synthesis. Polydispersity was until then a major hindering factor for colloidal crystal formation. Pusey et al. studied naturally occurring crystallization process and the phase behavior of hard sphere colloidal suspensions. In their work they mention for hard spheres the volume fraction where in crystal formation is seen ranges from 0.49 to 0.58.[5]

1.3 Recent literature review

1.3.1 Applications of colloidal crystals

Colloidal crystallization has been an active area of research since many years. Colloidal suspensions or colloids i.e. small particles suspended in a solvent with the particle size ranging from 10nm to 10^3nm, when self-organize in a long range periodic order form colloidal crystals.[1] During sedimentation a dilute dispersion forms dense sediment on the bottom of the solution. It is one of the simplest ways of colloidal crystallization but the process actually combines gravity settling, diffusion and crystallization in a complex way. [6]

The ordered colloidal crystals are being tested and have found wide-ranging applications in various fields. Colloidal crystals Bragg diffract light in specific wavelengths depending upon the lattice spacing and hence can be used as optical rejection filters[7] and optical limiters.[7, 8] The change in lattice parameters due to sensitivity towards the presence of some chemical species, leading to a change in diffracted light makes colloidal crystals potentially useful for applications like chemical sensors.[9] Periodic variation of dielectric constant in a colloidal crystal can create a photonic band gap while specific defects in the periodicity, leading to changing

properties of the photonic state, can act as wave-guides.[10, 11] Colloidal crystals have been used as a tool in studying the crystallization and melting phenomena.[5, 6] Understanding colloidal packing, film, stress and defect formation is also an area of interest.[12]

The enormous and promising application possibilities make colloidal crystallization and its control an important field of interest. In this context template directed colloidal self-assembly colloidal epitaxy becomes prominent due to its ability to direct, control and manipulate colloidal crystallization. There has been considerable work on colloidal crystallization using physical [13-36] chemical [37, 38] and optical [39] templates. Of the three, physical templates can give easy access to tune and scale the pattern dimensions when compared with chemical and optical templates.

1.3.2 Use of physical templates for colloidal deposition

Hard sphere colloidal particles, a simple colloidal system, under gravity settling crystallize into randomly oriented crystallites.[5, 6] On sedimentation, the negligible difference between face centered cubic (FCC) and hexagonal close packing (HCP) results in random close packing of the spheres but crystals grown slowly show a tendency towards FCC packing.[5] High rate of sedimentation greater than the maximum rate of crystallization produces a glassy state.[2] Temperature,[40] electric field[41, 42] and optical field[43] gradients have been used to control the rate of sedimentation for colloidal crystallization.

In their pioneering work, Blaaderen et al.[13, 14] have used FCC (110) lattice template to direct the crystallization of hard sphere like colloidal particles through slow sedimentation. For template fabrication, electron beam lithography was used to create a pattern similar to (100) plane of FCC crystal with holes comparable to the particle size, on a PMMA film with a thickness comparable to the particle radius. The observed FCC crystals were as large as the template and several thousand layers thick. In another approach the patterned template was made using one-dimensional pattern of lines with surface charge potential similar to that of the colloids. A meta-stable FCC crystal was

observed in a long-range repulsive interaction potential system. The pattern parameters in this system were tunable by varying the ionic strength and surface potential of the system.[15] Colloidal epitaxy was also used for growing hexagonally closed packed hard sphere colloidal crystals.[16]

Nagayama et al. have studied the 2D colloidal crystal formation on flat substrates under the influence of attractive capillary forces, convective transport of particles towards ordered region and controlled solvent/water evaporation rate.[17] In the template assisted self-assembly (TASA) method, Xia et al. used a special cell with a patterned bottom substrate.[21-23] The pattern on the bottom surface was generated by photolithography and etching techniques on silicon substrates. Using the patterned template and attractive capillary forces FCC colloidal crystals were created.[23] The patterns consisted of cylindrical holes, prism shaped holes, square rectangular templates and trenches. Using replica molding numerous similar templates were generated from the silicon templates. Xia et al. have suggested that the distance between two adjacent apexes of etched pits to be integral multiple of diameter for the generation of 100 planes.[24] Sequentially flowing different colloidal dispersions through the cell increased the complexity of the assembled aggregates.[25]

Ozin et al. have combined the methods of soft lithography and self-assembly to generate single crystal colloidal crystals in silicon wafers.[18] The 'V' shaped grooves were etched into a silicon wafer using a pattern defined on a PDMS master. The capillary forces drive the colloidal particles inside the groves and evaporating water dispersing agent close packs the particles inside the grooves forming a pattern of FCC crystal lines. Ozin et al. have also used the spin coating method to spread the colloidal suspension uniformly across the surface of a silicon template with etched square pyramidal pits. This method generated ordered and organized colloidal crystals parallel to the face of a single silicon wafer.[19] Using microspectroscopy Ozin et al. developed a 3D image of colloidal crystal formed on a glass template by capillary forces.[20] The pattern on glass substrates was made using soft lithography. Optical properties of these crystals were also studied using different size range of particles.

Colvin et al. have used the capillary forces and evaporating solvent to make colloidal crystals with controllable thickness on a flat micro slide using successive dip coatings.[26] Templates have also been used to create binary and ternary particle arrays and their inverted pore structure. In their work, Yang et al. have used V-shaped diffraction groove and replica molding to create PDMS patterned substrate for generating these arrays. In these experiments the spherical beads from the monodisperse colloidal suspension coated onto the patterned relief structure were driven into the V-shaped grooves by capillary forces. Binary and ternary particle arrays were fabricated by successive dip coating colloidal beads of different size onto the V-shaped arrays of micro spheres.[27]

Kumacheva et al. have used holographic gratings for patterning the positive photo resist coated anodes substrates for their experiments involving electrodeposition of particles against gravity. In their work small clusters confined in the physical geometries undergo structural rearrangements to produce close-packed crystals when the groove width is commensurate with the 2D lattice while incommensurability leads to non-close packed structures.[28]

Yodh et al. have used entropic forces and templates for generating colloidal crystal structures. The template structure creates localized and directional entropic force fields.[29] Maximizing the entropy in a binary mixture leads to an entropic attraction between the larger particles and between the particles and the wall.[30] Array of such walls or patterns was used to drive self-assembly of larger colloids.[33, 44] Using imprints techniques with an optical diffraction grating, a geometrical 1D and 2D template on 400nm PMMA layer was made. Different phases were observed in the 2D crystal with respect to the grating period on the template. The cross grating generated FCC crystal without stacking faults. The growth process was enhanced by high sphere concentration near the surface.[44] Yodh et al. have also used convective assembly scheme for the formation of a colloidal crystal through the evaporation of suspension solvent. 2D grating templates were used to grow the colloidal crystals. The square symmetry of the template was transferred to the colloidal crystal with the crystal thickness ranging to

about 50 layers. Templates were made using PDMS, adhesive only templates and adhesive with Au/Pd film. The growth was observed to be good in deeper regions of the pattern and it was suggested to match the particle size to the groove spacing. The particle concentration and crystallization was higher near the substrate.[32]

In other experiments involving template directed colloidal self-assembly, Shinya et al. have used ion beam irradiation for making electrified patterns on non- conductive surfaces. Micro sized particles were deposited selectively on the pattern from the particle dispersions in non-polar solvents. [33] Wiltzius et al. have used a square array of holes patterned on oxide coated wafers by photolithography followed by reactive ion etch as a template for colloidal crystallization using gravity settling.[34] Braun et al. have used focused ion beam lithography to make patterned templates.[35] Sedimentation of dilute binary suspension was studied using confocal microscopy. Point and line defects were seen due to mismatch between pitch of the substrate pattern and particle diameter.[35] Micro wells with micro magnet at the bottom of the wells have also been used to direct colloidal crystallization.[36]

1.3.3 Glass micromachining

Pattern fabrication on various kinds of glass substrates for microfluidic, microsensor or actuator applications has been a well-documented field. Wet etching of annealed glass slides using buffer oxide etchant with chrome and gold etch masks is a simple and widely used method of pattern fabrication on glass which can result in excessive undercut.[45] In a way to control the under cut various etch masks[46, 47] have been used which can reduce the undercut in the process to some extent. While presence of impurities does not effect the shallow etch profiles[48], presence of the non-SiO_2 components is known for the precipitate[49] and porous surface[50] formation during the wet etch process for multi-component glasses. Recent improvements to the process to address the problems include addition of hydrochloric acid to the buffer oxide etchant solution[51] or intermittent acid dipping[52] for removing the precipitate formed in glasses during wet etching processes.

Reactive ion etching techniques have also been studied for glass micromachining to some extent. Some of the parameters that effect the etch rate in this technique are power, gas species and flow rate as well as the substrate material.[53] The etch rate of glass increases with power[54] while presence of oxygen increases the etch rate.[55] It is well known that the glass composition greatly affects the micro fabrication process as sub-micron etching of different glasses was studied and reported.[54, 56, 57] Presence of non-SiO_2 components contributes to non-smooth etch of the glass while addition of heavy gases like argon improves the quality of etched glass due to increase in etch rates of non-volatile etch products in the process.[55] Deposition of non-volatile compounds due to the presence of atoms like Na, Al, Zn, Mg etc in the glass substrates effects the etch rate[54] as these compounds mask the glass surface and cause the transition from a process of chemical etching to physical etching.[58] This also adds to the lateral/side etching of the glass.[59] One of the studies on reactive ion etching of pyrex glass using nickel etch mask in CF_4/O_2 also indicate erosion of metal etch mask due to enhanced electrostatic field lines along the mask adding to the side/over etch of the pattern.[56]

Silica or glass substrates for colloidal epitaxy have been used by patterning them with reactive ion etching on thermal oxide layer coated on glass [34] and ion beam milling method for the glass coverslips.[35]

1.3.4 Ultraprecision machining of polymers

There has been considerable level of research in the machining of plastics to create micrometer size patterns. For ultraprecision machining of polymeric materials, poly(methyl methacrylate) is judged to be suitable plastic material for machining.[60] The variables which influence the machining of plastics include the tool design, tool spin speed and feed rate. Feed rate is the vertical speed of the tool.[61] Material properties of polymer materials also determine the quality of machining.[62] Elastic behavior of the polymer material, seen at high speed of cutting or milling when exceeds its yield points results in cracks along the polymer surface.[60] While machining, when temperature of polymer exceeds the glass transition temperature, then a smooth profile is observed.[62] PMMA (laminated or molded) machining using computer numeric control machines

with a diamond cut tool generally reaches the glass transition temperature for PMMA to give smooth profiles.[62] The surface roughness on cut PMMA is reported to be least.[60] Ion milling can be used for tool fabrication followed by machining on PMMA with pattern dimensions in the range of 25μm in depth and height to give low surface roughness in the machined sample at high tool rotation speed.[63]

PMMA substrate has been used in colloidal crystallization experiments, patterned using electron beam writing[13] and diffraction grating imprint method.[32]

1.4 Summary of conclusions

In this research an attempt was made to create templates conforming to confocal microscopy requirements while utilizing the photolithography, glass micromachining and mechanical ultraprecision machining methods.

A simple etch recipe developed in this research was used for patterning of thin glass cover slips. Three different metal masks were used in this research while selecting nickel as suitable etch mask for the process. Glass being a multi-component substrate, the etch process was modified by using a intermittent acid dipping to remove the non-volatile products from the reactive ion etch process which effect the etch rate of glass substrates. Erosion of metal etch mask was seen in this case which also contributed to side etch of the patterns.

For mechanical fabrication of polymeric templates, computer numerical control machining (CNC) was used for creating patterns in a highly controlled manner. Speed of cut and repeated machining were the two variables in the machining process. One of the limitations of the method was availability of smaller cut tool sizes, which also determine the size of the pattern being fabricated. A 50μm radius of curvature and 90° engraving cutter tool was used in the machining experiments. The pattern of holes from these experiments had considerable surface roughness.

The microfabricated physically templated surfaces were used for colloidal deposition experiments and colloidal structures thus formed were observed using

confocal scanning laser microscopy. Particles under go self-assembly in the geometrical confines of the pattern under the influence of gravity and capillary forces from drying. Limited order in particle arrangement was seen using confocal microscopy. Detailed description of the packing of colloidal particles with in the confines of the template pattern was obtained by combining confocal microscopy images and a simple modified Fortran code for image writing and reading to generate images of particle packing in different view planes.

2. EXPERIMENTAL

2.1 Microfiche mask preparation

Microfiche can be used as a simple and easy photomask for photolithographic purposes.[64] The micrometer size patterns on microfiche in this research were fabricated using a two-step process. In the first step the desired pattern was created using Microsoft paint as a bitmap file. The size of the file was adjusted to a width of 9600 pixels and height of 12600 pixels. Single pixels width lines were created in sets with single to four-pixel size separation between each line of each set respectively. The length of the lines varied from 100 to 200 pixels. Similarly array set of dots of single pixel size was created with single to four-pixel separation between each dot of respective sets. This file was then printed on a 1200 dots per inch printer on an 8.5”x11” paper in the scale to fit mode. In the second step the printed image was sent for commercial 20x size reduction on to a microfiche (Health Science Center, Texas A&M University).

A single pixel from 9600x12600 size bitmap file when printed on 1200 dots per inch printer would create a single dot equal to 20 micrometers approximately. A further size reduction generates 1μm size of features. The confocal image of microfiche (Figure-2.1) showed the width of lines to be around ~12μm, which was about 10 times larger than expected. The distance of seperation between two adjacent lines was at the maximum of 4 pixel separation was about 40μm and for one pixel separation it was about 12μm. The holes on the microfiche were particularly underdeveloped. The dark field mask was created in microfiche so as to use positive photoresist to create the desired pattern features. Positive photoresists are capable of pattern transfer with the best possible resolution.[65] The microfiche can be used to generate photoresist patterns in the range of 10μm, with edge roughness on the microfiche to the order of ~1μm.[64]

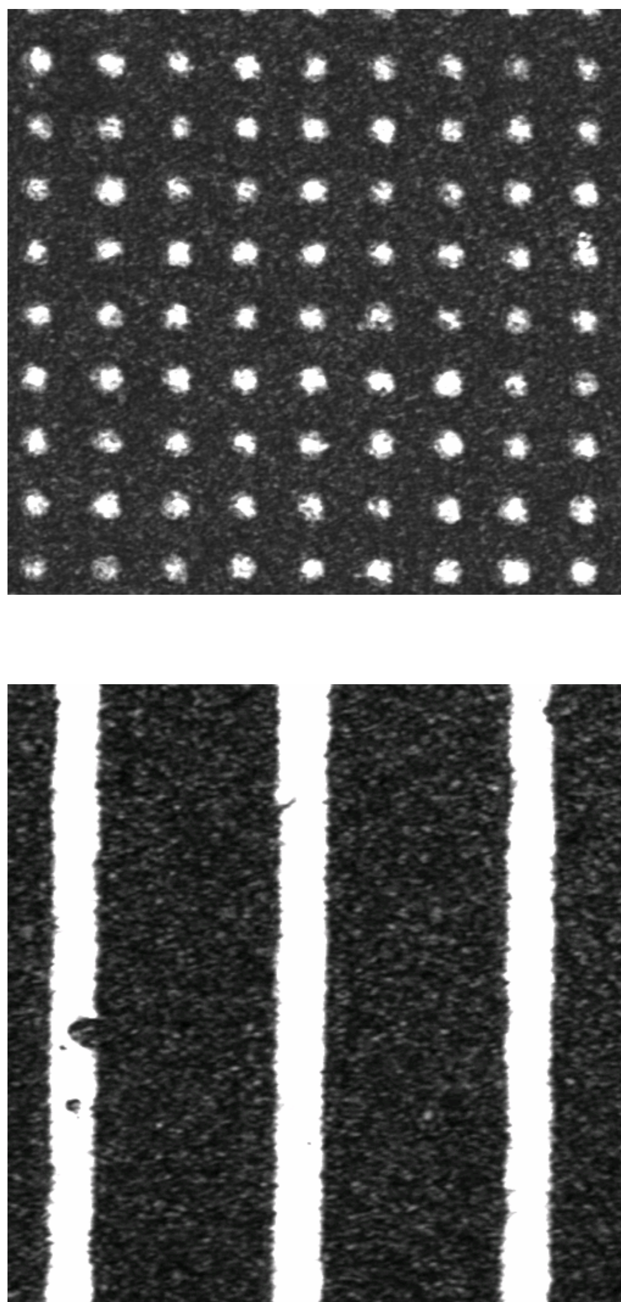

Figure 2.1. Pattern on microfiche. Top image: Pattern of holes undeveloped on the microfiche. Bottom image: Pattern of lines on microfiche. Pattern size or width on microfiche ranged between 10-12μm.

2.2 Glass substrate preparation

Thin corning zinc titania glass cover slips from Corning, were used as principal substrates in photolithography related experiments. Borofloat glass substrates were also used for analyzing the effect of glass composition on the etch rate and profile (Table-2.1). The basic process is summarized in figure 2.2. The substrate is prepared using metal and photoresist deposition. After ultraviolet photolithography and metal layer etching, the pattern is transferred to the glass substrate.

In this process, the glass coverslips are washed in deionized water, micropore liquid soap, deionized water and acetone in that order. The cleaned cover slips are immediately dried in nitrogen flow. These cover slips are then heated on a hot plate at a temperature of 100°C for 2 minutes to make the surface water-dry. The coverslips are then loaded in a metal deposition chamber for depositing metals, which are used as etch masks in the fabrication process. The pressure at the beginning of the deposition is set at least at 2×10^{-6} torr. The metal source is heated using a resistance heater and an external power supply. As the material source becomes hot, atoms of vapor are generated which move straight up towards the substrate surface to form a thin metal film.[65] The deposition rate of the metal is controlled at 0.1-0.3nm per second while adjusting the current in the range from 4 to 6 amperes. Low pressure and low rate of deposition are essential for good metal layer adhesion and coverage,[65] which is important especially during dry etching. Rotation of the substrate holder improves the coverage of the thin metal film on the substrate surface.[66]

Table 2.1. Types of glasses used in experiments.

S.no	Type of glass	Thickness mm	Composition
1.	Zinc-titania glass, Corning 0211.	0.15-0.17	SiO_2 64%, B_2O_3 9%, ZnO 7%, K_2O 7%, Na_2O 7%, TiO_2 3%, Al_2O_3 3%
2.	Borofloat glass, Precision glass).	~1	SiO_2 80.6%, B_2O3 13%, Na_2O 4%, Al_2O_3 2.3%

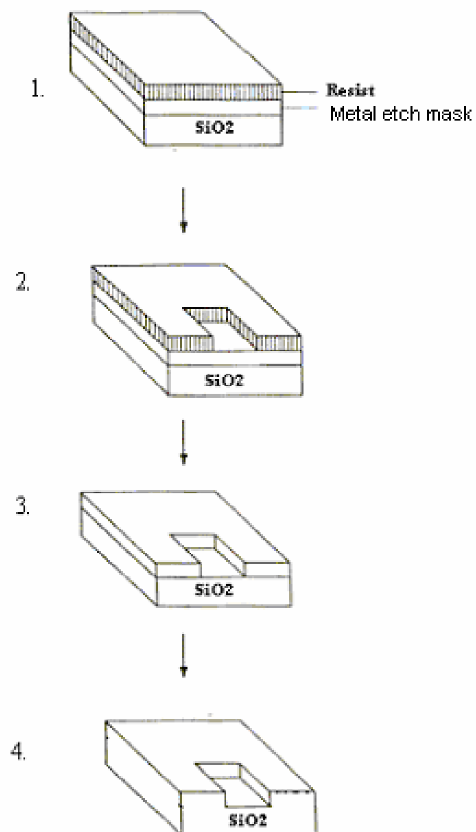

Figure 2.2. Steps in glass substrate patterning. 1. Photoresist and metal layer coated on the glass cover slip. 2. Photoresist development. 3. Metal etching and development. 4. Glass etching and pattern transfer using either wet etching or reactive ion etching..

For metal deposition, commercial Nickel wire (99% purity, Alfa Aesar) is used which was wound around a tungsten rod (Alfa Aesar). Commercial chrome rods (99% purity, Alfa Aesar) were used for chrome metal deposition and for aluminum, commercial pellets (99% purity, Alfa Aesar) were used in a tungsten boat (Alfa Aesar). The tungsten rod and boat serve as resistance heater for heating the metal source. Four sets of samples were prepared using these metals (Table 2.2).

Table 2.2. Etch masks description.

Sample set	Metal layer	Metal thickness-nm	Etchant	Etch mask for technique
1.	Chromium	75-100	CR-7	Wet and Dry etching
2.	Aluminum	100	Solution-2	Dry etching
3.	Nickel	70-80	CR-7	Dry etching
4.	Chromium + Nickel	5+ 75 and 50+75	dil. Aqua regia followed by CR-7	Dry etching

Note: CR-7 : 9% $(NH_4)Ce(NO_3)6$+6%$HClO_4$+H_2O
Solution-2, (Aluminum etchant) : 80% H_3PO_4+5%HNO_3+5% CH_3COOH

2.2.1 Photolithography

A mask aligner (Quintel, CA) was used for photolithographic techniques. Metal-coated cover slips were used in this part of the experiments. A 2µm layer of positive photoresist (Shipley 1827, MicroChem) was spin coated on the cover slips at a speed of 3000rpm for 40 seconds. The spin-coated photoresist was then soft baked on hot plates for 2 minutes at 100°C and at 120°C for another 2 minutes to dehydrate and drive off all solvent from the photoresist layer. The photoresist is then UV exposed for 25 seconds and developed in the positive developer solution for 60-90 seconds (Figure 2.3).

The sample is then dried in N_2 flow followed by heating at 120°C to ensure strong adhesion between the photoresist and the metal layer.[65] The metal layer is then etched in a metal etchant solution (see table 2.2 for etching solutions). The metal layer is etched until the glass transparency is visible.

2.2.2 Wet etching

Glass micromachining using wet etching techniques is a widely used method for glass patterning. The wet etching involves three-step process, which included the movement of etchant to the surface of the glass, chemical reaction on the surface and

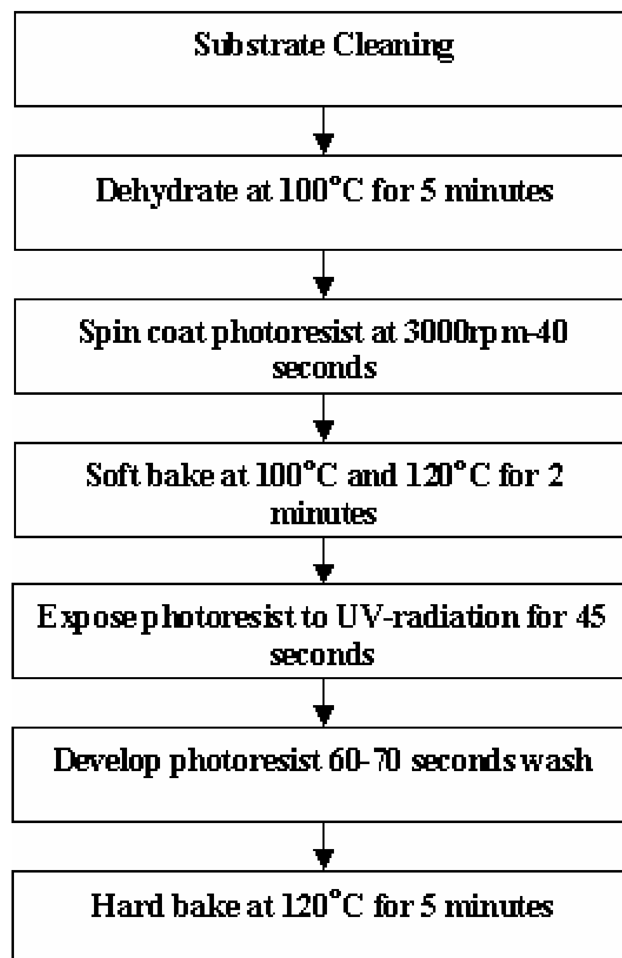

Figure 2.3. Steps in ultraviolet photolithography.

movement of the product away from the glass surface to expose more glass for further etching.[67] The wet etching experiments in this research were all done at room temperature and in an ultrasonicator for agitation. Agitation increases the movement of etchant and products into and away from the surface respectively.[67]

Buffered oxide etch (BOE) is an etching solution which is a mixture of 99% HF and 40% NH_4F in water at various proportions. In this research HF: NH_4F at 1:20, 1:10 and 1:5 ratios were used for etching corning 0211 glass coverslips. HF and NH_4F were purchased from Aldrich. Chrome coated coverslips were used for etching in BOE. For the protection of the uncoated glass cover slip side, an adhesive tape was attached which was later removed after etching and the side was cleaned in soap, deionized water and acetone. The sample was then dried in nitrogen stream. The overall reaction for the SiO_2 etch process is given by,

$$SiO_2 + 6HF \rightarrow H_2 + SiF_6 + 2H_2O$$

NH_4F is added to buffer the solution, maintaining constant HF concentration.[65] Wet etching is a completely isotropic process and typical etch profiles show a flat bottom with curve walls for an etched sample.[45] Due to undercut problems involved, wet etching is not preferred for etching features 2μm or less.[65] For long duration of etching or at high HF concentrations photoresist does not act as a good etch mask for wet etching process. Chrome layer can be used as etch mask for the process but this does not avoid undercutting in glass. Borosilicate glasses are known to etch faster than SiO_2.[52] The impurities present in the multi-component glasses form insoluble compounds during the etch process. Compounds like CaF_2, ZnF_2 etc. deposit on the surface of the glass during deep etching and hinder the etch rates of glass.[51, 52] Precipitates[49] and rough surface formation[50] during etching is attributed to the presence of these impurities. Two recent improvements to this process have addressed these problems by including dilute HCl in the process. Addition of HCl in the etchant solution or intermittent 1M HCl wash[51, 52] during BOE etching process improves the etch rate as well as the etch surface. The HCl forms water soluble chlorides with the metal fluoride and can be washed away

in water before proceeding with the wet etching. Thermal annealing of glass slides before etching is also an important step, which improves the surface quality of the etched sample.[45]

2.2.3 Reactive ion etching

Reactive ion etching is based on the principle of generation of high-energy chemically reactive neutrals and ions, accelerated under the effect of electric or magnetic fields towards a target substrate.[65] The gas molecules collide with high-energy electrons produced in the process and generate the reactive species, the directionality of the energized species gives the anisotropy character to the etching process.[65] Glass is etched using CF_4 +O_2 chemistry (Figure 2.4). The chemical etch mechanism of SiO_2 in CF_4+O_2 plasma is expressed as[55]

1. $CF_3(g)+SiO_2 \rightarrow CF_3(ads)+SiO_2$
2. $F(g)+SiO_2 \rightarrow F(ads)+SiO_2$
3. $CF_3(ads) +SiO_2 \rightarrow C (ads)+3F(ads)+SiO_2$
4. $4F(ads)+Si(s) \rightarrow SiF_4(g)$
5. $SiF_4(ads) \rightarrow SiF_4(g)$
6. $C(ads)+xO(s) \rightarrow COx(ads)$ x=1 or 2
7. $COx(ads) \rightarrow COx(g)$

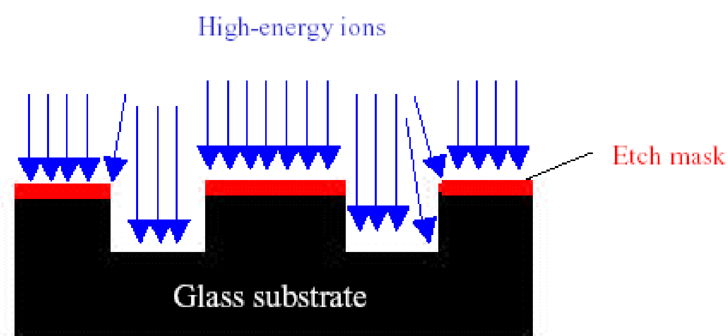

Figure 2.4. Schematic for reactive ion etching.

Reactive ion etching consist both physical as well as chemical reactions; positive ion bombardment at the surface in physical reaction where as SiO_2 is removed as SiF_4 through chemical reactions.[53] The four key steps involved in the process are surface adsorption of etchant species, chemical decomposition of the species on the surface, chemical etching reactions and the desorption of the products and the byproducts from the surface.[55] Important factors which influence the etch rate include gas flow rate, flow ratio of gases, pressure, power and substrate material.[53-55] Low pressure with high ratio of CF_4/O_2 flow rate and high power is known to create good etching conditions for glass.[68] The etch rate increases with power as more energized molecule form during the etch process while low pressure increases the directionality in the etch process as molecules have more time to access substrate surfaces for etching.[65] High rate of oxygen reduces the etch rate as it competes with CF_4 for occupying SiO_2 surface and thus inhibiting reaction.[55]

Other gases which have been used for the etch process include CF_3, and SF_6[54, 59] and CF_4/Ar[53] where Ar contributes to physical etching. For multi-component glasses, impurities like B_2O_3 form volatile products with fluorine chemistry where as Na_2O, CaO, ZnO, Al_2O_3 etc form metal fluorides, which get deposit on the glass surface and these impurities effect the etch rate as they reduce the contact between the etchant species and glass surface.[54] Some of the problems in the etch process arise from the etching of the etch mask leading to trenching where there is preferentially excess etching

at the corners of the etch mask.[66]

Reactive ion etching was used as a process for developing maximum possible anisotropic structures on glass coverslip. After pattern development on the resist and the metal layers, reactive ion etching method is used in a flow of CF_4 and O_2 at varied gas flow rates, power values and etch duration. CF_4 source was purchased from Praxair and the reactive ion etch chamber was March CS 1701. In this process, corning 0211 coated with Cr, Ni, Al and Ni on chrome layers and borofloat coated with Cr were used for etching purposes. In the etching experiments the coverslips were attached to a microscope slide with adhesive tapes to provide support and stability in the etching chamber.

The photoresist layer is etched away in the process while the metal layer acts as a etch mask. After the process, the coverslips is removed from the slide and the metal layer is completely etched away in metal etchant. The sample is then washed again with deionized water followed by drying in nitrogen flow. Intermittent 1M HCl wash was attempted on the sample undergoing reactive ion etching to possibly obtain an anisotropic etch profile on the coverslip glass.

2.3 Mechanical machining

In this part of research, mechanical machining of polymeric templates is considered for creating patterned polymeric templates. The substrates were spin coated poly(methyl methacrylate) (PMMA) layers, which were about 10 to 15µm thick. PMMA is known for its suitability in ultra precision machining.[62] A 20%, 30% and 35% PMMA solution was prepared using toluene as solvent. The solution is made in 5 hours or more of continuous ultrasonication. Spin coating was done at 500rpm and 1000rpm. The layering of two or more PMMA layers was done to obtain 10-15µm layer thickness of pmma. Samples were heated at temperatures 50 °C and/or 150 °C.

For mechanical machining computer numerical control machine (Roland CNC co.) was used. The substrate holder was a 9cm x 4cm x 2.8cm solid wax. Small holes of 1 cm and 2mm diameter were made in the wax body for routing the vacuum supply. The

wax body was firmly held on the CNC platform using 2 screws. A simple pattern with lines separated by 100μm and 8x3 point array with each point separated by 100μm was made using "dr. engrave" software. The CNC cutting tool, carbide cutter (microcutusa), had a radius of curvature of 50μm and tip angle of 90°. The speed of cutting of the carbide cutter on the polymer substrate was varied while using a one step cut depth of 10μm. The surface and cut profile were observed using confocal microscope.

2.4 Confocal microscopy imaging experiments

Using confocal microscopy images can be obtained with high precision from different focal planes as the laser scans through the bulk. The Confocal scanning of templates and colloids is done using a LSM 5 pascal, Zeiss confocal microscope. Rhodamine with 10^{-4} M concentration in Glycerol, dimethylformaldehyde (DMF) or immersion oil solution is used as a refractive index matched fluorescent liquid for the experiments as and when specified. For imaging, the pattern with maximum line separation was scanned in all the patterns and comparisons were made for the etch profiles seen in this case. The colloid packing related experiments with polystyrene were mostly done using immersion oil solution, which has a refractive index value of 1.52. A 80μl volume of colloidal suspension is used on the substrates and allowed to dry in 3-4 hours. A small drop of immersion oil is used for scanning the samples.

Polystyrene particles of size 4μm and 6μm were purchased from duke scientific. 1μm Silica particles were purchased from polyscience. Confocal microscopy involves refining some of the imaging parameters for better scanning of the sample. The pinhole size was fixed at a value of 100 for all the images. Pinhole diameter relates to the depth of focus for the scanning laser and small pinhole diameter decreases the light intensity received from the focus while increasing the depth of focus. The aperture blocks light from other points while imaging a well defined spot on the sample.[69] 543nm HeNe laser was used at an excitation level of 80. The laser excites the fluorescent dye to a detectable color allowing high resolution in scanned sample.[70] Fluorescence medium is used in order to obtain color-differentiated clear particle images. Fluorescent

differentiates the solution from the presence of particles or other bodies which appear in dark in these experiments. 63X objective was used for imaging the particles. For the latex particles when scanning is done in immersion oil, the sample is scanned with in 30 minutes as the latex particles begin to dissolve in the oil. For PMMA, DMF was avoided as it acted a solvent for the PMMA material.

Images are generated as a stack, which was later, manipulated by a simple Fortran code. A stack of images were created with X: Y: Z size in ratio 1:1:1 in three coordinates. The numbers of slices in the image stack were chosen to obtain complete depth of the view, ranging to a depth of about 20-25μm for the image features, which was enough to get the complete profile of 4-8μm big feature sizes. Interval between each plane of depth on scan adjusts with the scale on X:Y plane so that the XYZ voxel has identical dimensions. Only variables adjusted to optimize the image quality correspond to the value of the detector gain, amplifier offset and gain. Detector gain adjusts the light intensity for the photomultiplier and this is followed by optimization of image clarity by adjusting the amplifier gain for brightness and amplifier offset for black level in the background.[69] The detector gain is varied around 500 as the numerical value.

With silica particles, index-matching glycerol with rhodamine was used to obtain fine images. For further improvement immersion oil was used on the dry samples instead of the glycerol solution. A zoom of 3 to 4, was used to obtain magnified images of the particles in the patterns. Refractive index matching is important in order to reduce the scattering of laser light while traversing from different media.

The samples after etching tend to be rough due to the etching process, either during wet etching where the etchant attacks through the metal etch mask in long duration of etch or in dry etching where the high energy sputtering effects the substrate layer beneath the etch mask surface. The roughness might affect quality of images during confocal imaging of the samples. The best imaging was possible on glass substrates with silica particles in glycerol solution or polystyrene particles in immersion

oil solution either on glass or on PMMA pattern feature with a glass bottom. Silica particles in glycerol on PMMA also gave fairly good images

In the next step, the image stack from confocal imaging is converted to tagged image file stack. The image size was restricted to 512x512 pixels. Fortran code, which converts the stack into three-dimensional matrix, is modified to produce two additional plane views apart from the side views of the plane it produces along the image length (Figure 2.5). Modified code created image stack along the image width in a plane perpendicular to the stack and also along the diagonal of the stack. The code involves reading and writing manipulation of the image matrix.

For the first view plane, the code collects information along the XZ plane while stacking the image planes along Y direction. Similarly the process is repeated for YZ plane with stacking along X direction. For diagonal view the image information along the diagonal lines of XY image plane is stacked as a plane, recreating the diagonal plane image. These images can be stacked from one edge to the other end of the XY plane. Diagonal planes end or begin at odd pixels along the Y direction due to ensured continuity in the plane stack. For each diagonal stack plane the dark regions are evenly distributed in either sides. Along the diagonal view, the lateral dimensions are around 30% lower than the true value.

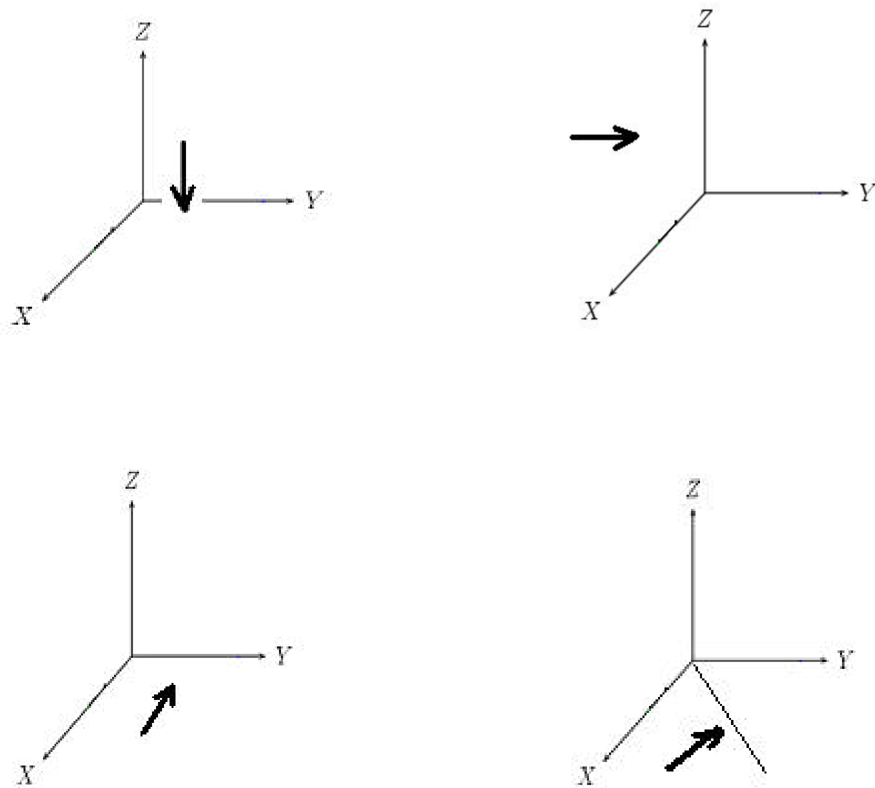

Figure 2.5. Fortran image processing: View planes from Fortran imaging. Images arranged clockwise from top: XY planes stacked along Z-axis, XZ planes stacked along Y-axis, planes along the XY plane diagonal and ZY planes stacked along X-axis.

3. PHOTOLITHOGRAPHY AND GLASS MICROMACHINING FOR PHYSICAL PATTERNING OF TEMPLATES

3.1 Introduction

In this part of the research ultraviolet photolithography and glass micromachining methods are extensively used for patterning thin glass cover slips with structures of micrometer dimensions (Figure 3.1). The cover slips used in this research are essentially a multi-component type of glass. The non-SiO_2 components in the glass make it difficult to achieve directional etching in glass. Exploration of an effective etching technique for glass cover slips is important in the context of their suitability in confocal microscopy related experiments and more importantly due to the fact that general glass cover slips are far less expensive and easily available when compared to quartz cover slips.

An attempt is made for developing a suitable etch recipe to control the under cut and facilitate anisotropic etching of thin glass cover slips. Dry etching or reactive ion etch is compared with and preferred over wet etching techniques due to the possibility of directional etching of glass and comparatively low undercut. Different protective metal etch masks and etch parameters were used during the dry etching of the cover slips to find the effective process method.

Etch rates and profiles of etched glass in different etching conditions is observed, determined and compared using confocal microscopy which is a simple and quick way with in the experimental requirements of this research that is substrate thinness and transparency. Attempts were also made to optimize the etch process parameters to obtain minimum under cut and maximum anisotropy. The profiles of interest as observed during the process include general curved wall with planar bottom from wet etching techniques, ellipsoidal and near vertical etch from reactive ion etch in glass.

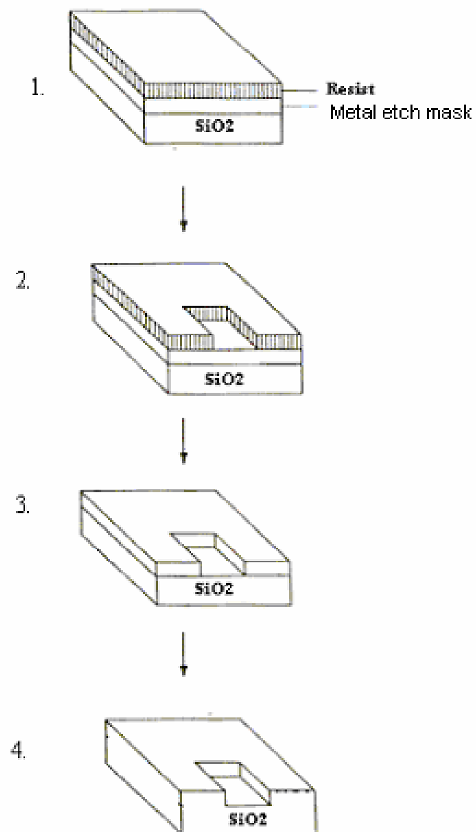

Figure 3.1. Steps in ultraviolet photolithography pattern transfer. 1. Photoresist and metal layer coated on the glass cover slip. 2. Photoresist development. 3. Metal etching and development. 4. Glass etching and pattern transfer.

3.2 Experimental

3.2.1 Materials

Glass coverslips (corning 0211 zinc titania glass) were used as substrates for this part of the research. Microfiche with printed patterns was used as a photomask. Nickel wire, aluminum pellets and chrome rods were purchased from Alfa Aeser to be used as etch masks for the process. Metal etchants were prepared and used for chrome, nickel and aluminum etching (see chapter 2 for details). Shipley 1827 positive photoresist and positive resist developer was used for the photolithography purposes. Wet etching solution for glass was prepared using buffer oxide etchant i.e. ammonium fluoride and hydrofluoric acid (NH_4F:HF) in 5:1, 10:1 and 20:1 ratio. For dry etching carbon tetra fluoride and oxygen gas mix (CF_4+O_2) etchants were used in a reactive ion-etching chamber.

3.2.2 Substrate preparation procedure

The glass substrate was cleaned initially either in soap, deionized water and acetone or cleaned in nichrome mix and in the final stage it is dried in a nitrogen stream. Four different sets of samples were prepared using chrome, nickel and aluminum metal deposition (see table 3.1). Only set 1 was used in wet etching while all the sets were used in dry etching. The metal deposition was done in a deposition chamber at a rate of 0.1 to 0.35nm and at a starting pressure of 2 or $3x10^{-6}$ torr. Shipley 1827 photoresist was spin coated on the cover slips and exposed to ultraviolet light. The pattern was developed in the resist developer and later the metal layers were etched in the specific metal etchant solutions.

Table 3.1. Metal etch masks description.

Sample set	Metal layer	Metal thickness-nm	Etch mask in technique
1.	Chromium	75-100	Wet and Dry
2.	Aluminum	100	Dry
3.	Nickel	70-80	Dry
4.	Chromium + Nickel	5+ 75 and 50+75	Dry

The metal layer beneath the photoresist is etched in the exposed regions after the photoresist development. The etching is done until the glass surface can be seen. The solutions for metal layer etching were prepared as discussed in chapter 2. For chrome and aluminum it takes less than 2 minutes while for nickel it can take about 10 minutes of slow etching in chrome etching solution and around 5 minutes in dilute aqua regia.

The pattern is then transferred to the glass substrate using etching techniques. Wet etching has been used for pattern fabrication on glass substrates in applications like patterning micro fluidic channels.[45, 51, 52, 57] The general method of wet etching glass is using buffered oxide etch or BOE. Three different ratios of BOE were used for etching cover slips and etch rates and etched profiles were observed in confocal microscopy. The three solutions used had 1:20, 1:10 and 1:5 (HF: NH_4F) BOE etchant concentration respectively. All the samples were wet etched in an ultrasonicator for about 60 minutes. The backside of the coverslip was protected using an adhesive tape, which was later removed after the completion of etching process. The chrome layer was used as an etch mask for glass coverslips in this process.

In order to obtaining less undercut while etching glass coverslips, reactive ion etching an anisotropic process was also attempted. It involves chemical etching and physical bombardment of ions or species acting simultaneously on the target material. Generally about 8% of O_2 is used along with CF_4 for SiO_2 etching.[71] In this research the glass coverslip being multi-component glass a different etch recipe is attempted to obtain

almost anisotropic patterns in the etched sample. Cover slips with metal etch masks were used in this part of research. While CF_4 attacks the SiO_2 and also contributes to physical etching by bombardment, O_2 helps in increasing the etch rate by making more fluorine species available for the process while forming carbon dioxide with carbon molecules from the plasma.[56, 72] Oxygen molecules also etch the substrate through physical bombardment.[55] The other parameters which influence the process include power, etch gas flow rate, pressure and substrate characteristics.[53] The important parameters that were manipulated in this process include etchant gas concentration ratio, flow rates and power applied in the process. Pressure was always kept low at zero reading and was determined by gas flow rates in the chamber. The Effect of different protective metal masks was also investigated. In these experiments the coverslips were attached to a microscope slide for stability and support while etching in the reactive ion etch chamber.

3.2.3 Etch rate and profile determination using confocal microscopy

For confocal microscopy, glycerol solution with 10^{-4} M Rhodamine was used. A 50µl drop of approximate refractive index matched solution was used on the sample and was later scanned using confocal microscopy. Side views were generated to obtain cross section of etch profile on glass. Etch rates were hence determined in each case by dividing total etch depth obtained with total etch duration.

3.3 Results and discussion

3.3.1 Ultraviolet photolithography

The ultraviolet photolithography experiments were done by varying the exposure time for the positive photoresist. Shipley 1827 was used for the experiments; spin coated to give 2-3µm resist thickness. The photoresist is selectively exposed to ultraviolet light and the exposed regions are dissolved in a developer solution leading to transfer of pattern on to the substrate. The positive photoresist usually are the choice for better pattern transfer using photolithographic methods.[65]

Optimum duration of photoresist exposure is important for good pattern transfer.[66] For the pattern 25-second exposure was observed to be optimum in terms of reduced roughness of the edges for the pattern transfer in case of the lines. This exposure duration was used in all of the photolithography experiments in this research (Figure 3.2). Pattern development on resist is done with a 60-90 seconds wash in photoresist developer and the sample is then heated at 120°C for 5 minutes to hard bake the photoresist layer and increase the adhesion with the glass substrate. The pattern of line and holes in the microfiche were varied in width and some roughness of edges was inherent all through the pattern components. The holes were particularly under-developed for the 25 seconds optimized exposure. The pattern on microfiche shows non-uniform size and shape of holes, which was also hence seen in the photolithographic pattern transfer process.

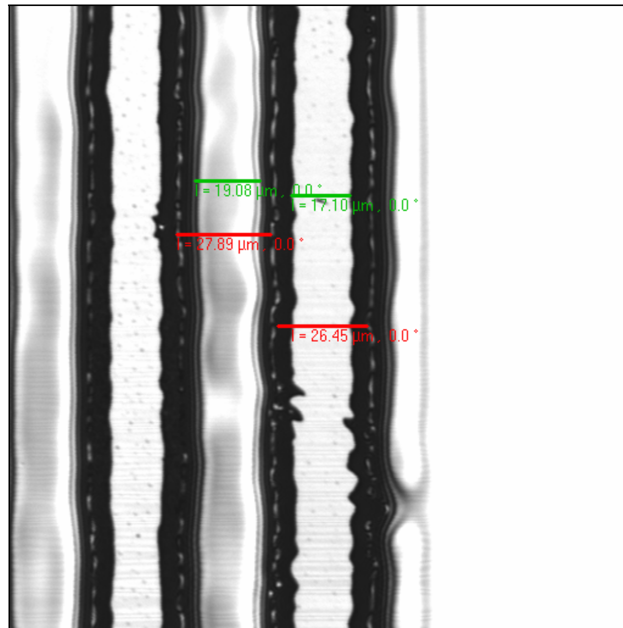

Figure 3.2. Pattern on photoresist after 25 seconds of UV exposure.

3.3.2 Wet etching

For long duration wet etching photoresist is not known to survive long in the ultrasonicator and hence the chrome etch mask was used for the purpose. In the etch process, the concentration ratio of the BOE effects the etch rate of silicon dioxide.[73] Wet etching techniques create undercut which can be as large as 200% of original size for 10μm size width with etch depth of 10μm.[45] Increasing the concentration of HF in the BOE increased the etch rate of glass and as can be seen also added to the undercut as shown in figure 3.3, figure 3.4 and figure 3.5. Experimental conditions are summarized in table 3.2. Curved profiles can be seen in each of the cases which is characteristic of glass etching due to the isotropic nature of the etch process.[45]

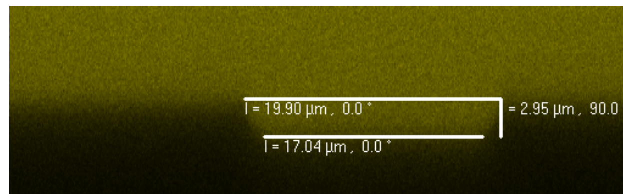

Figure 3.3. Etch profile of coverslip etched in 1:20 BOE for 60 minutes. (sample 3.3).

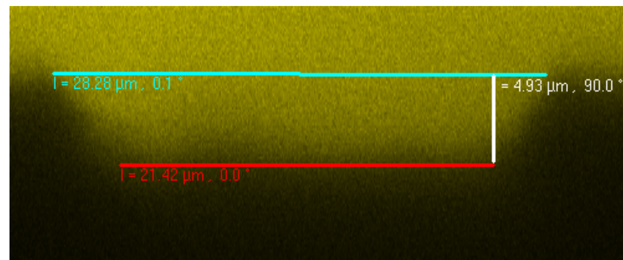

Figure 3.4. Etch profile of coverslip etched in 1:10 BOE for 60 minutes. (sample 3.4).

Table 3.2. Wet etching : Summary

Parameters	Samples		
	3.3	3.4	3.5
Substrate	Corning 0211	Corning 0211	Corning 0211
Etchant ($HF:NH_4F$ ratio)	1:20	1:10	1:5
Time	60min	60min	60min
Metal mask	Chrome	Chrome	Chrome
Difference between top and bottom sides (µm), D	2.86	6.86	11.9
Vertical depth (µm), H	2.95	4.93	8.47
Etch rate, µm/min	0.05	0.082	0.14

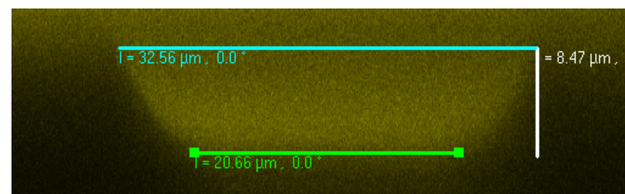

Figure 3.5. Etch profile of coverslip etched in 1:5 BOE for 60 minutes. (sample 3.5)

3.3.3 Reactive ion etching

The factors explored in the reactive ion etching of glass coverslips included the selection of suitable etch masks and effective process parameters. The effects of etchant gas flow rates and their ratios along with the power applied for the process were analyzed to some extent in order to obtain usable patterns on the glass substrate.

Metal etch masks are important for limiting the etching process only to the desired locations. Polymer resist are etched away in the experimental conditions and fail to prove reliable for the purpose and hence metal masks like chrome have been used as etch masks in reactive ion etching techniques when pattern depth in few micrometers is desired.[68] Chrome has low etch rate in plasma and hence can be used as an etch mask for reactive ion etch processes with CF_4 and O_2 chemistry.[73] In the following experiments a 150-200nm thick chrome layer was used as etch mask. It was observed during the experiments that chrome layer did not survive for more than 30 minutes of etch. Also the etch pattern produced within 30 minutes of etch was not perfect as shown in the figure 3.6. The two long dips at the edges of the pattern were seen almost every time after etching. Figure 3.6 shows the pattern profile for the etched glass with the process parameter specifications for SiO_2 etch. Few of the possible reasons for the long narrow trench formation were investigated. It is known that thermal annealing improves the surface profile for glass in wet etching process. The cover slips were thermally annealed by heating the sample to a temperature of about 480-500°C for 2 hours. As can be seen in figure 3.7, the annealing of the sample did not solve the dip formation problem.

The reasons for dip formation could be attributed to the mask erosion and hence an effect similar to trenching[65] or some reaction chemistry involved in the process leading to the formation of the dips. Contour and reverse etching of chrome oxide films have been reported with CCl_4+O_2 as etch gases due to the presence of tungsten oxide as impurities.[74] Reverse etch was also reported in the same study. A similar problem of groove formation near etch mask edges was mentioned in the case of soda lime glass with aluminum mask and the reason was attributed to increased AlF_4 concentration near edges in the presence of O_2.[53] Based on a similar assumption the sample was etched in pure CF_4 but problem was not solved (Figure 3.8). Experimental conditions are summarized in table 3.3.

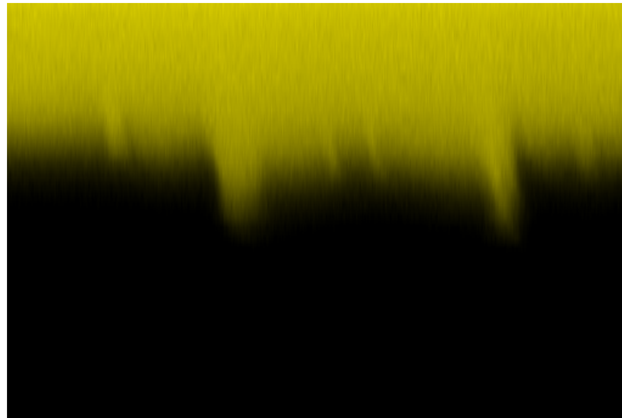

Figure 3.6. Reactive ion etching of corning 0211 with chrome etch mask, $CF_4:O_2$ at 14:2 flow rate and etched for 15 minutes at power P=200W. Two trenches at the edges and low etch in the glass can be seen. (Sample 3.6).

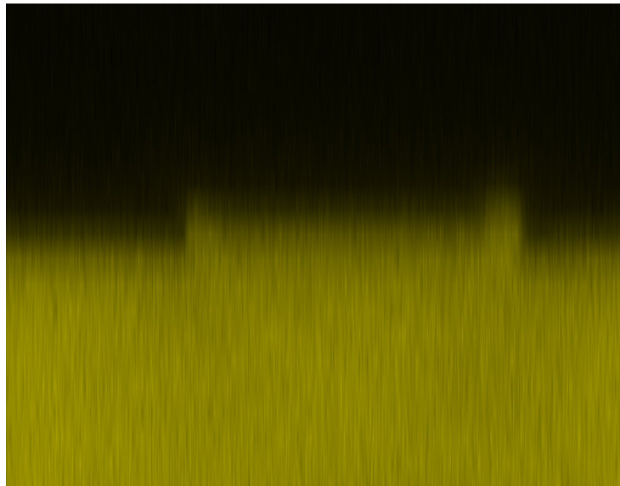

Figure 3.7 Annealed corning 0211 with chrome etch mask. Glass etched in similar conditions as sample 3.6. (Sample 3.7). Image is up side down from confocal imagining.

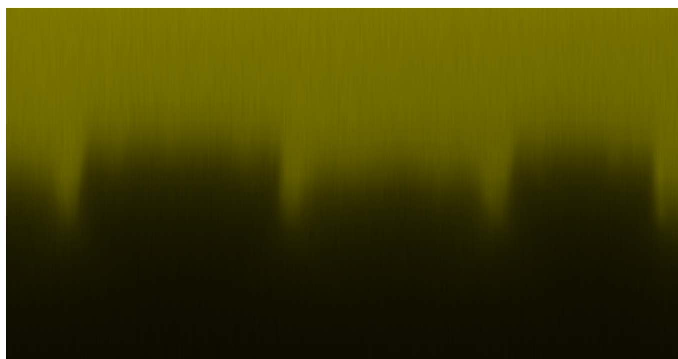

Figure 3.8. Corning 0211 glass with chrome mask, etched in 100% CF_4. At 200W and 14 standard cubic centimeter per minute (sccm) flow rate. (Sample 3.8).

Table 3.3. Dry etching with chrome etch mask

Parameters	**Sample**		
	3.6	3.7	3.8
Substrate	Corning 0211	Corning 0211 (Annealed)	Corning 0211
Etchant CF_4:O_2 flow rate ratio (sccm:sccm)	14:2	14:2	14:0
Power P	200	200	200
Time, min	15	15	15

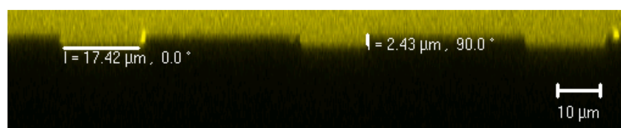

Figure 3.9. Etch profile of borofloat glass. Total gas flow rate of 16 sccm, CF_4:O_2 at 14:2 flow ratio. Glass etched at P=200W for 15 minutes.

In the next step the substrate was changed to Borofloat micro slides. Similar etch profile was not seen in borofloat glass which is a multi-component glass with 80% SiO2 concentration, (Figure 3.9).

The cover slip contains about 35% of non-SiO_2 contents. Most of the constituents form non-volatile compounds during the etch process and deposit on the etch surface effecting the etching rate.[54] In an effort to improve the etch profile by removing the impurities to get more sensible pattern, a 5 minutes of etch was followed by 15 seconds of 1 M HCl and 15 seconds of HF etch. The results show the tendency of undercut and existence of dip pattern creating non-planar pattern profile, (Figure 3.10).

Figure 3.10. Etch profile of corning 0211 glass with chrome as etch mask and intermittent acid wash. Total gas flow rate of 16 sccm in CF_4:O_2 at 14:2 flow ratio. Glass etched at P=200W for 15 minutes. Intermittent wash with 1M HCl and 15 seconds of HF etch after every 5 minutes. Cycle repeated 3 times. Confocal image is up side down.

Aluminum metal coating was used as etch mask for coverslip samples. The coverslips were etched under the same conditions as the chrome layer coated samples (Table 3.4). The formation of uneven profile was seen in these samples, (Figure 3.11). In the next step aluminum was etched in 100% CF_4 where the edge dips weren't seen explicitly on the etched profile, (Figure 3.12). However, again like chromium, aluminum coating did not completely survive the 30 minutes etching duration. The surface film was extensively blackened and etched.

Nickel is also known to survive in the reactive ion etching process[57] and proved to be a better etch mask in this research. No side dents similar to chrome or aluminum masks were seen in this case under similar etching conditions (Figure 3.13) but high undercut was seen in the etching process making the process less anisotropic. Attempts were made to control the undercut in this case by varying the parameters like gas concentration and power.

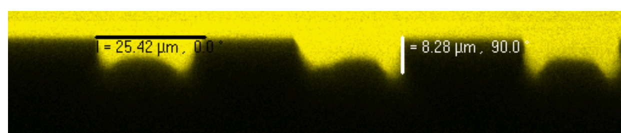

Figure 3.11. Reactive ion etching of corning 0211 with aluminum etch mask. Trenches along the edges can be seen in the above image. CF_4:O_2 at 16 sccm flow rate at 14:2 ratio and power P=200W. (Sample 3.11).

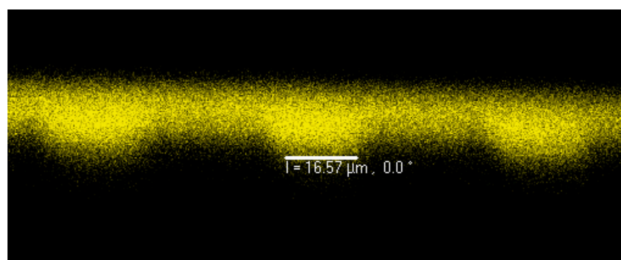

Figure 3.12. 100% CF_4 and aluminum etch mask. The damage on the surface of glass with aluminum etch mask due to erosion of Al in 100% CF_4 RIE made imaging difficult. No clear trenches can be seen. Etching conditions:14 sccm gas flow rate at P=200W. (Sample 3.12).

Table 3.4. Dry etching with aluminum etch mask

Parameters	**Sample**	
	3.11	3.12
Substrate	Corning 0211	Corning 0211
Etchant CF_4:O_2 flow rate ratio (sccm:sccm))	14:2	14:0
Time	30min	30min
Metal mask	Al	Al

In attempts to control the under cut the etching was also done at various etch gas flow rate ratios using nickel etch masks. As a reference the etch recipe similar to for pure SiO_2 was applied at a flow rate of 16sccm of etch gases. The variation of etch gas ratio and its effect on the etch process is reported. Figure 3.13 and 3.14 show profile for etching conditions at high CF_4 to O_2 ratio.

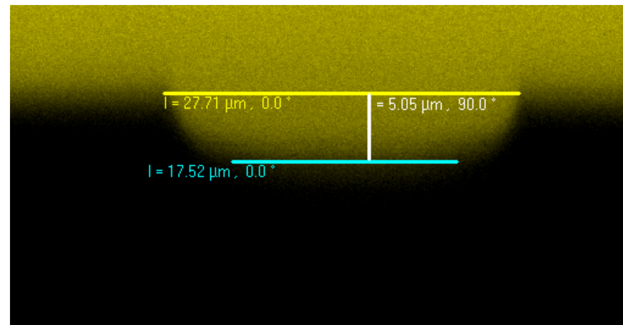

Figure 3.13. Effect of gas flow ratio on etch profile: CF_4:O_2 at 14:2 flow rate ratio. 30 minute etch at P=200W. (Sample 3.13).

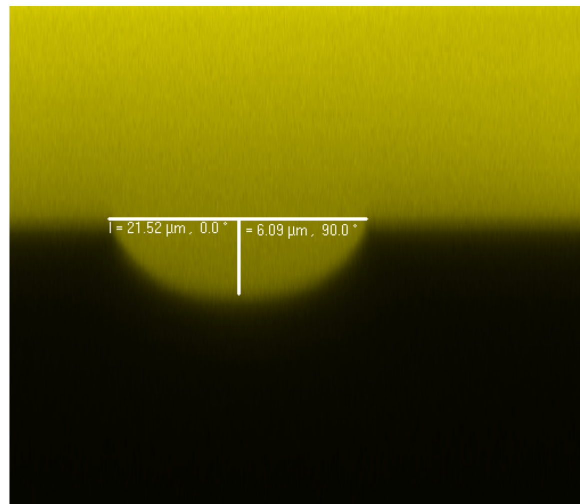

Figure 3.14. Effect of gas flow ratio on etch profile: CF_4:O_2 at 8:8 flow rate ratio. P=200W, 30 minute etch. (Sample 3.14).

Figure 3.15 and 3.16 show etch profiles at low CF_4:O_2 ratio. Low ratio resulted in low etch rates.

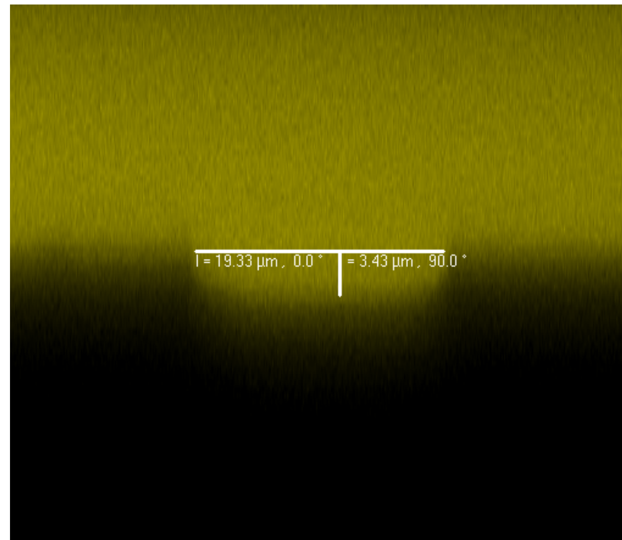

Figure 3.15. Effect of gas flow ratio on etch profile: CF_4:O_2 at 4:12 flow rate ratio. P=200W, 30 minute etch. (Sample 3.15).

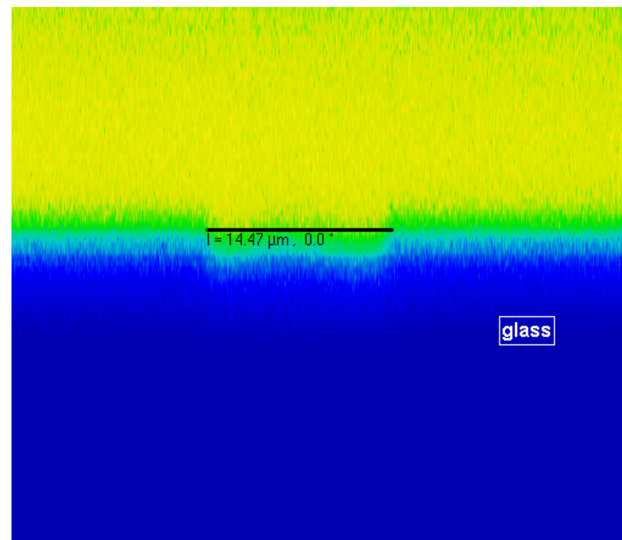

Figure 3.16. Effect of gas flow ratio on etch profile: CF_4:O_2 at 2:14 flow rate ratio. P=200W, 30 minute etch. Blue region in the flase color image above is the glass substrate. (Sample 3.16).

Generally CF_4 etches the SiO_2 and forms volatile fluorine products while O_2 makes the fluorine more available by preventing recombination with carbon species.[55] The etch rate initially increased probably due to more availability of fluoride plasma ions to etch the glass and then decreased with the CF_4 gas concentration (Table 3.5). Also the undercut was seen to decrease making the profile more anisotropic. The decrease in etch rate can be attributed to lesser CF_4 concentration to etch the glass and while increasing concentration of oxygen might also increase the directional physical bombardment with the substrate material along with CF_4.[55]

Table 3.5. Etch gas flow ratio and glass etch rates.

Parameters	**Sample**			
	3.13	3.14	3.15	3.16
Substrate	Corning 0211	Corning 0211	Corning 0211	Corning 0211
Etchant CF_4:O_2 flow rate ratio (sccm:sccm)	14:2	8:8	4:12	2:14
Power P	200	200	200	200
Time, min	30	30	30	30
Metal mask	Nickel	Nickel	Nickel	Nickel
Vertical depth (μm), H	5.05	6.09	3.43	1.7
Etch rate, μm/min	0.17	0.203	0.104	0.056

The CF_4 primarily attacks the silicon dioxide in the glass and converts it to volatile SiF_4. It removes SiO_2 through the chemical attack and makes the process directional under the influence of the power in the process chamber.[55] The gas flow rate increase tends to add to isotropic etching as excess CF_4 molecules might attack the edges or exposed glass surface and side walls Figure. The amount of etchant flow rate was reduced to 10 sccm in order to limit the excess etchant flow. The ratio of CF_4 to O_2 was made 3:7 to increase the anisotropy of the etched profile, (Figure 3.17). The power was kept at 200W.

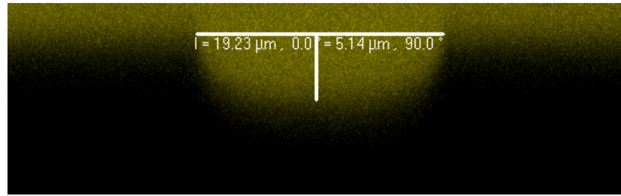

Figure 3.17. Coverslip etched at an etch gas flow rate of 10sccm with 3:7 ratio of CF_4:O_2 at 200W. Low etch gas flow rate and high oxygen rate was preferred to control the chemical reactions and hence the undercut on the sample.

Most of the experiments were done at a power of 200W. Low power produces less energetic plasma which effect the etch rate due to decreased physical bombardment.[55] At low power no etch was detected and as the power is increased the etch rate can be seen to increase. Profiles under different power while keeping the CF_4:O_2 gas rate at 14:2 and etch time at 30 minutes, are shown in figure 3.18 to 3.22.

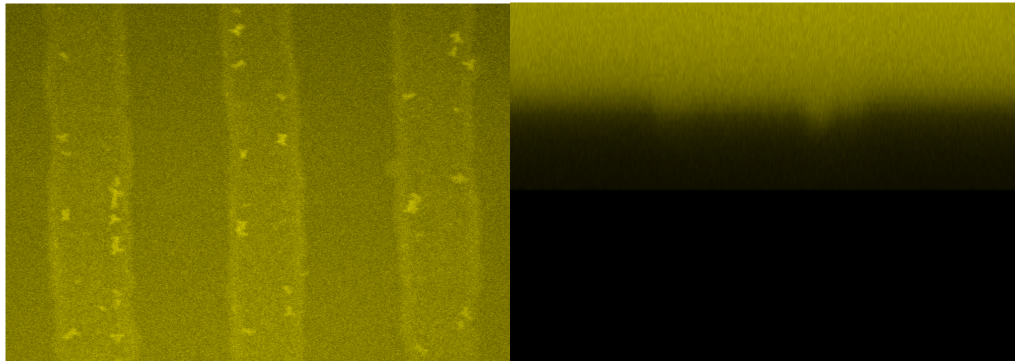

Figure 3.18. Effect of power on etch rates: P=100W. CF_4:O_2 at 14:2 sccm and etch duration is 30 minutes. (Sample 3.18). (Left image: top view, right image: cross sectional view).

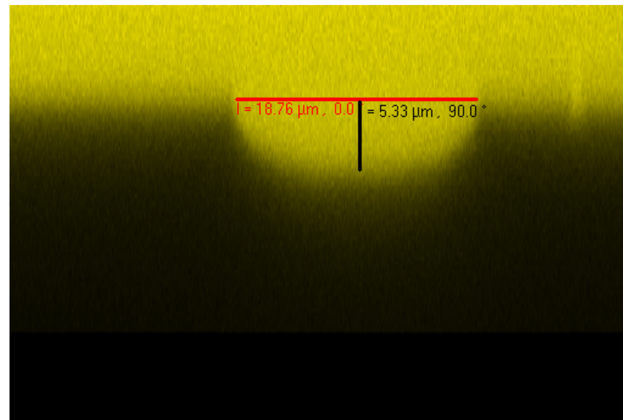

Figure 3.19. Effect of power on etch rates: P=150W. CF_4:O_2 at 14:2 sccm and etch duration is 30 minutes. (Sample 3.19).

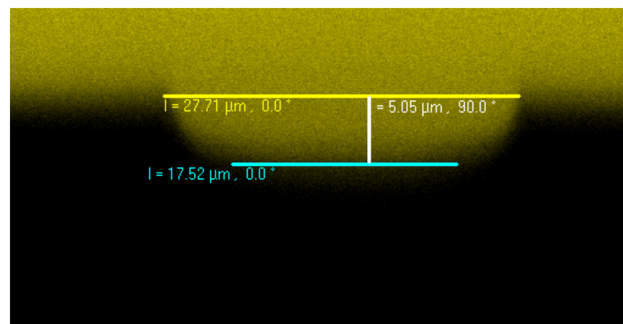

Figure 3.20. Effect of power on etch rates. P=200W. (Sample 3.20).

High power increases the etch rate and also effects the etch mask. Beyond 200W, at 250W and 300W as can be seen the pattern has embedded holes which were made through the etch mask (Figure 3.21 and 3.22). Experimental conditions are summarized in table 3.6.

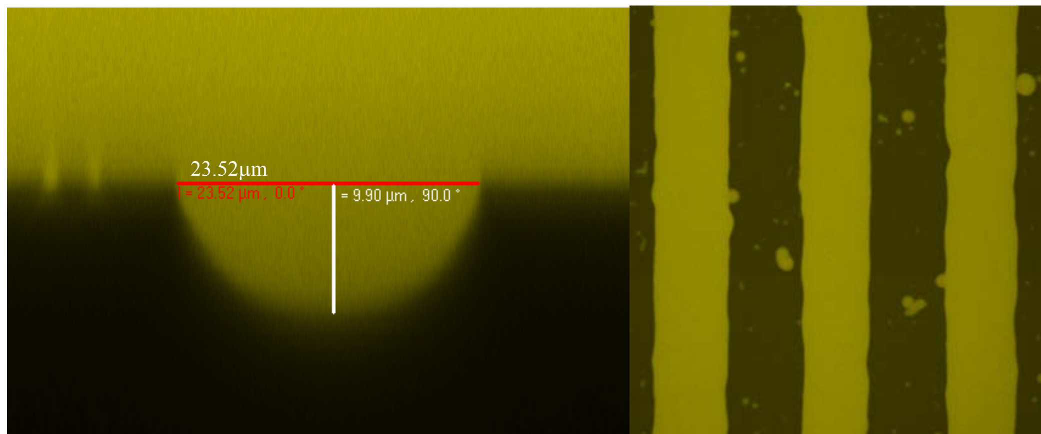

Figure 3.21. Effect of power on etch rates. P=250W. (Sample 3.21). Formation of holes on the surface due to nickel layer etch in high power. (Left image: cross sectional view, right image: top view).

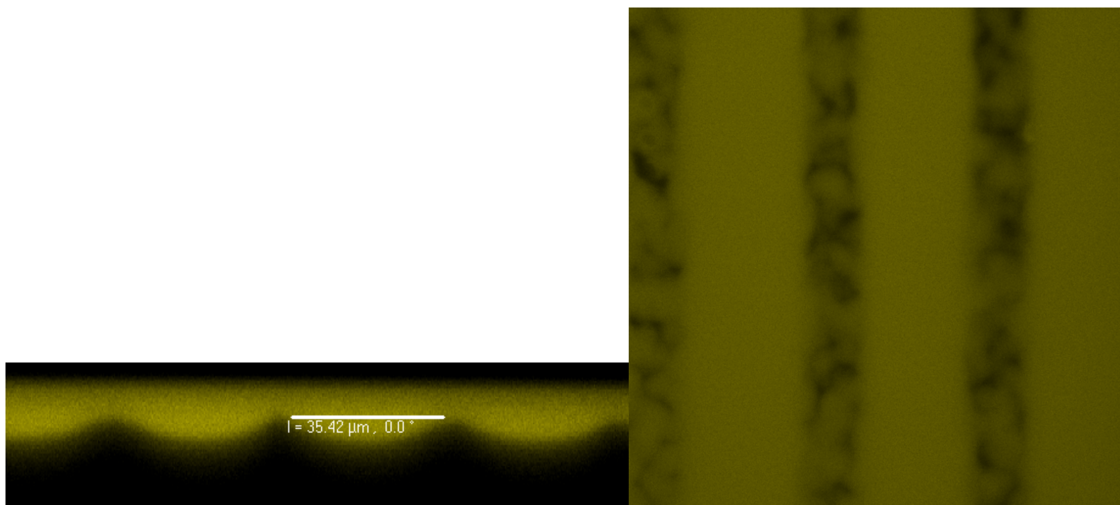

Figure 3.22. Effect of power on etch rates. P=300W. (Sample 3.22). The excessive surface damage due to etching of the etch mask itself at high power. (Left image: cross sectional view, right image: top view).

Table 3.6: Effect of power on etch rates.

Parameters	**Sample**				
	3.18	3.19	3.20	3.21	3.22
Substrate	Corning 0211	Corning 0211	Corning 0211	Corning 0211	Corning 0211
Etchant CF_4:O_2 flow rate ratio (sccm:sccm)	14:2	14:2	14:2	14:2	14:2
Power P	100	150	200	250	300
Time, min	30	30	30	30	30
Metal mask	Nickel	Nickel	Nickel	Nickel	
Vertical depth (μm), H	-	5.33	5.05	9	-
Etch rate, μm/min	-	0.174	0.168	0.3	-

One important observation to note in these experiments is that in corning 0211, non-volatile components constitute about 30% of its content which might also be one of the factors hindering anisotropic etch of glass cover slip. As the duration of etch was doubled under similar etching conditions, a relative increase in depth was not seen instead the under cut increased (Figure 3.23). This can be explained possibly in terms of non volatile products which are not etched away in the process[54-56] covering the surface, though no surface analysis was done in this case. A simple 12 second 1 M HCl wash followed by wash in DI water was used to remove the non-volatile products after a 5 minutes reactive ion etch step. The undercut was significantly controlled with the combination and inclusion of these modifications in the process (Figure 3.24). Experimental conditions are summarized in table 3.7. Similar steps were reported in wet etching of soda lime glasses to remove unsolvable impurities in wet etching to increase the etch rate.[52] In the reactive ion etch, this step increased the etch rate and the under cut was also reduced.

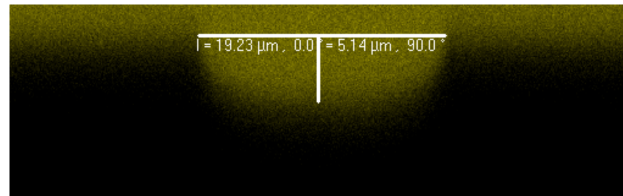

Figure 3.23. Corning 0211 etch profile for 30 minutes RIE. P=200W with low CF_4:O_2 etch gas flow rate at 10sccm with 3:7 ratio. (Sample 3.23).

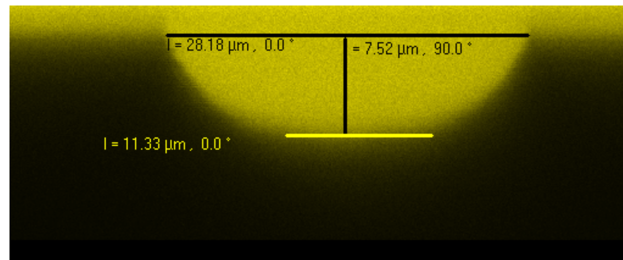

Figure 3.24. Corning 0211 etch profile for 60 minutes Etching for 60 minutes. Experimental conditions similar as for sample 11.a. Image shows increase in undercut. (Sample 3.24).

Table 3.7: Effect of duration of etch.

Parameters	Sample	
	3.23	3.24
Substrate	Corning 0211	Corning 0211
Etchant CF_4:O_2 flow rate ratio (sccm:sccm)	3:7	3:7
Power P	200	200
Time, min	30	60
Metal mask	Nickel	Nickel
Vertical depth (µm), H	5.14	7.52
Etch rate, µm/min	0.171	0.125

The etch profile of substrate shows erosion of nickel mask in the intermittent process of etching as the step profiles in the images show (Figure 3.25 and 3.26).

Similar erosion was reported in earlier works where it was attributed to increased electrostatic line fields, which might affect the nickel layer.[56] In order to prevent the increased electrostatic field, thick resist was recommended. The problem lies in survival of Shipley 1827 photoresist in these experiments beyond 5-7 minutes in the reactive ion etch process. No dents at mask edges were seen intermittent HCl after every 15 minutes of RIE, (Figure 3.27) though there was undercut and less anisotropy compared to sample 3.25 and 3.26. Etching conditions are given in table 3.8.

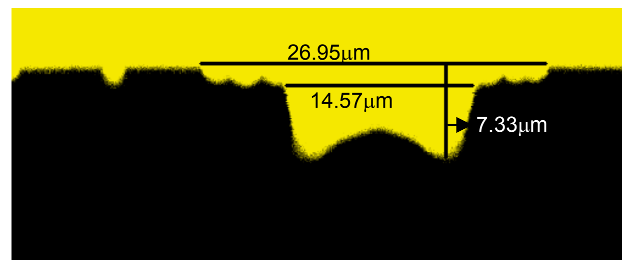

Figure 3.25. Corning 0211 etch profile for 30 minutes RIE, 5 minutes intermittent HCl wash, nickel mask. 3:7 CF_4:O_2 flow rate at 10 sccm, 200W, 5 minute intermittent HCl wash to remove non-volatile impurities. Large long trenches around the edges of etched channel might be the result of mask erosion which can be seen on the top of the glass surface near the edges. (Sample 3.25).

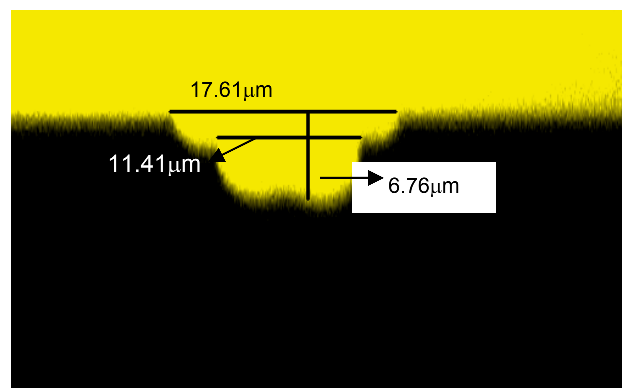

Figure 3.26. Corning 0211 etch profile for 30 minutes RIE, 10 minutes intermittent HCl wash, nickel mask. 3:7 CF_4:O_2 flow rate at 10 sccm, 200W. 10 minute intermittent 1M HCl wash shows erosion of nickel near the edges. (Sample 3.26).

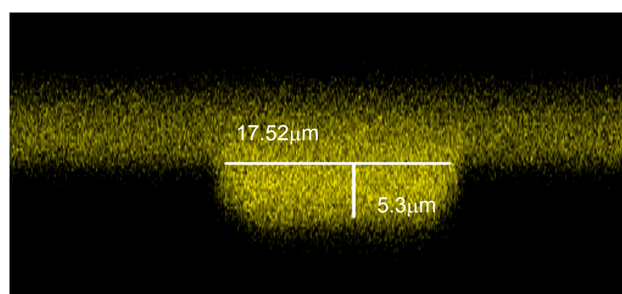

Figure 3.27. Corning 0211 etch profile for 30 minutes RIE, 15 minutes intermittent HCl wash, nickel mask. 3:7 CF_4:O_2 flow rate at 10 sccm, 200W. 15 minute intermittent HCl wash shows reasonable etch profile. (Sample 3.27).

Table 3.8: Effect of intermittent HCl wash on corning 0211 glass etch rate and profile

Parameters	**Sample**		
	3.25	3.26	3.27
Substrate	Corning 0211 (annealed)	Corning 0211	Corning 0211
Etchant CF_4:O_2 flow rate ratio (sccm:sccm)	3:7	3:7	3:7
Power P	200	200	200
Time, min	30	30	30
Metal mask	Nickel	Nickel	Nickel
Intermittent HCl wash	After every 5 minutes	After every 10 minutes	After every 15 minutes
Vertical depth (μm), H	7.05	6.76	5.33
Etch rate, μm/min	0.235	0.225	0.177

Prevention of mask erosion was attempted using a thin layer of chrome which is regarded as a good adhesion provider in wet etching.[45] The etching process was done with etching parameters (table: 3.9) and with set 4 which is cover slip coated with a 5nm chrome and 75nm nickel mask. The profiles are shown in the figure 3.28 to 3.30. The problem of pattern side etching or contour etching was seen again in this case similar to pure chrome etching process.

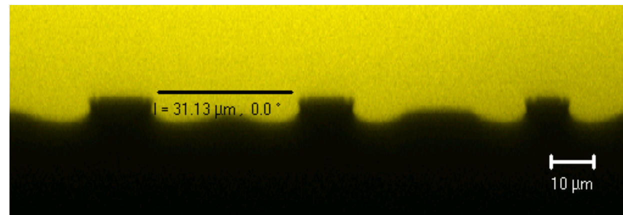

Figure 3.28. Etch profile with chrome adhesive layer. Chrome was used to prevent the nickel erosion. Trenches were etched excessively in this case. Side view of the pattern profile. (Etching condition in table 3.9). (Sample 3.28).

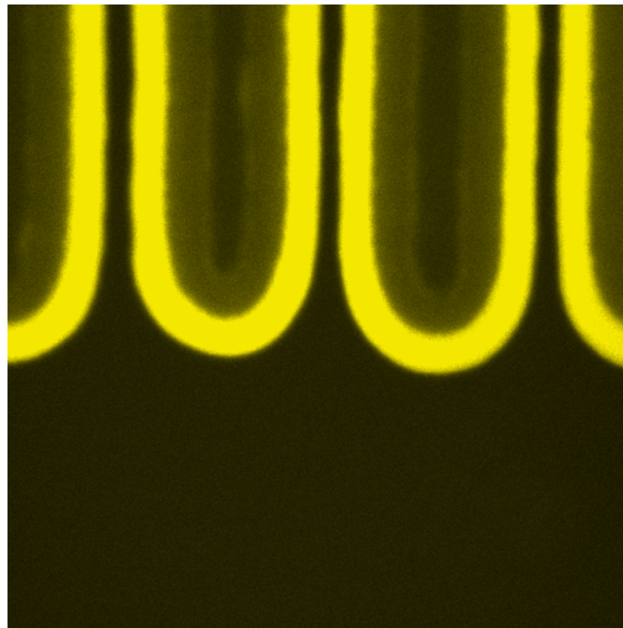

Figure 3.29. Top view of the sample with chrome layer as adhesive metal for nickel mask. The bottom most layer shown in yellow fluorescence. (Etching conditions in table-3.9).

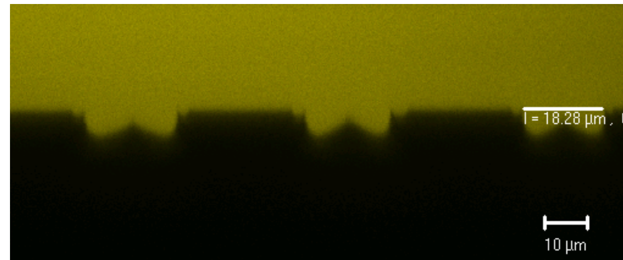

Figure 3.30. A 5nm chrome adhesive layer and nickel etch mask still resulted in trenching and mask erosion. (Etching conditions in table 3.9). (Sample 3.30).

Table 3.9: Effect of chrome adhesive layer

Parameters	**Sample**	
	3.28	3.30
Substrate	Corning 0211	Corning 0211
Etchant CF_4:O_2 flow rate ratio at 10sccm (sccm:sccm)	3:7	3:7
Power P	200	200
Time, min	30	30
Intermittent HCl wash	After every 10 minutes	After every 10 minutes
Chrome+Nickel thickness nm	50+75	5+75

The pattern etch steps was then changed to 15 minutes for intermittent wash and the profiles can be seen in figure 3.31. The simple HCl wash step increased the etch rate while also decreasing the undercut issue for the substrate to some extent.

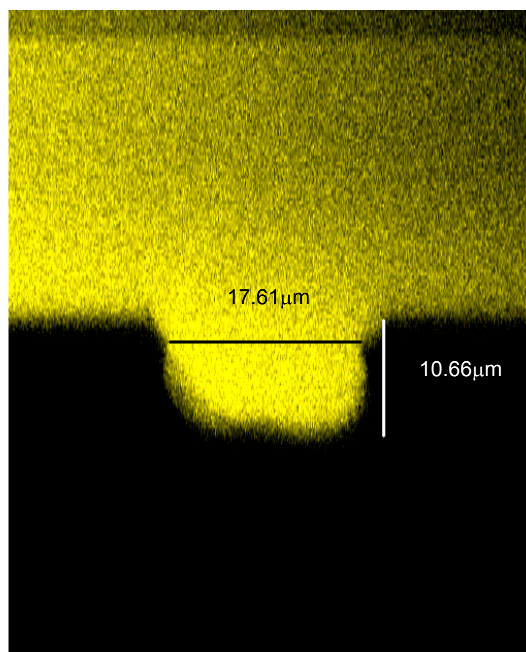

Figure 3.31. Corning 0211 etch profile with intermittent 1M HCl wash after every 15 minutes for total 45 minutes of RIE. 7:3 ratio of CF_4:O_2 at 10sccm (standard cubic centimeter per minute) flow rate, 200W power. Etch mask used is nickel.

3.4 Conclusions

Using standard photolithography techniques, pattern transfer was done on metal-coated glass coverslips. The multi-component glass etching was attempted using nickel as protective mask, which proved to be a good etch mask for reactive ion etching. Chrome and aluminum etch mask were not useful for the purpose due to high trenching seen at the edges of the etch mask. For the etch process the etch gas flow rates and power was varied and 200W power was optimum for the process. In order to remove the non-volatile compounds formed on glass during the etching process an intermittent 1 M HCl wash followed by washing in deionized water was attempted. Etching was continued after the wash and isotropic etch was controlled to some extent in this process as observed using confocal microscopy. The erosion of nickel mask was seen in the process. Optimized HCl wash after 15 minutes of reactive ion etching was attempted and structures on coverslips were fabricated with low undercut and increased anisotropy.

4. PATTERNING OF TEMPLATES BY MECHANICAL MACHINING OF POLYMERIC FILMS

4.1 Introduction

In this section of the research, the focus is on patterning polymeric templates, using mechanical machining methods to utilize them later for colloidal deposition experiments. The choice of polymer material for this part of the research was limited by the conditions of its suitability in confocal microscopy experiments and its machinability. Confocal microscopy requires the substrate thickness to be in few hundred micrometers while also being optically transparent. Poly(methyl methacrylate), a low refractive index polymeric material, was used as template material in this part of the research. The standard photolithographic processes for patterning poly (methyl methacrylate) are costly as well as time consuming.[63] As an alternative, the patterning of spin coated PMMA films is attempted using computer numerical control machining, (CNC), which is a common mechanical machining technique.

Ultraprecision machining of PMMA using CNC has the potential of being a simple fabrication method for patterning of templates with a greater control on machining parameters and pattern design. Simple to complex patterns can be created on variety of work pieces using CNC machines with computerized stage and tool control.[75] Ultraprecision machining of blocks or laminates of plastics using diamond tip tool show PMMA to be a suitable material for machining with the capability of obtaining negligible surface roughness.[60-62] Machining of PMMA workpieces using specially fabricated micromilling tools can give micrometer size patterns with small size and shape deviation.[63]

The important factors that influence the machining process include the machine stage stability, machining parameters and the physical properties of the substrate material.[62] In terms of machining conditions, when the depth of cut is made too large cracks appear around the drilled holes and in case the depth of cut is too small at high

spin speeds, excessive heating of the material can cause shape distortion.[61] In terms of the material properties, it is important that while cutting, the material reaches the glass transition temperature for smoother cut profiles.[62] PMMA behaves like a ductile material for long ranges of cut parameters to give smooth profiles.[60-63]

In this research, with in the limitations of the machining conditions, machine parameters were varied to obtain simple and usable patterns. A 50μm radius of curvature, 90° engraving cutter was used for the purpose. The substrate used was a 10-15μm thick PMMA layer spin coated on a glass coverslip. Attempts were made to fabricate a small array of holes as deep as the film thickness while optimizing relevant machining parameters using CNC machining. Refractive index matched solution was used on the pattern to observe pattern profiles using confocal microscopy. High surface roughness and large cut size and cracks were seen in most of the holes created with different sets of machining parameters including the least vertical cut speed combined with maximum spin speed. It is important to note that the pattern size scale reduction will depend on the machining tool size. It will be necessary to obtain relevant size tools to down scale the size of the pattern features.

4.2 Experimental

4.2.1 Materials

Glass coverslips (corning 0211 zinc titania glass) were used as a base for spin coating PMMA layers. Poly(methyl methacrylate) (MW 120K) was purchased from Aldrich. Toluene (histological grade) from Fisher scientific was used as solvent for PMMA solution. For machining purposes, one of the smallest size of cutters available, a 90° degree engraving carbide cutter with a 50μm radius of curvature, was purchased from Microcutusa. CNC machine used in the research was from Roland CNC co. A P-6000 spin coater from specialty coating systems was used for spin coating the cover slips with PMMA.

4.2.2 Substrate preparation procedure

The glass substrates were cleaned with soap, deionized water and acetone followed by drying in nitrogen stream. Three concentrated solutions of PMMA dissolved in toluene were prepared with 20%, 30% and 35% PMMA by weight. Three different sets of samples were prepared using these solutions. For spin coating experiments, the samples were flooded on the coverslips and spin coated at different speeds and/or multiple times while ensuring good polymer coverage on the sample. At least 10µm thick polymer was desired as per the minimum cut tool depth limit of the CNC machine. Slow acceleration to ensure uniform spreading was applied by manually tuning the spin speed at 20-50rpm/s to the desired maximum speed. All the sets were spin coated for about 45 seconds. The samples were then heated at 50°C for 10 minutes or/and followed by 10 minutes heating at 150°C as specified. Heating in 2 steps was done for solvent evaporation and annealing to smoothen the surface of the sample.

4.2.3 PMMA machining

The spin-coated samples were placed on a supporting platform. The support was made using solid wax, 9cm x 4cm x 2.8cm in dimensions. Wax being a soft material will not damage the tool tip during any accidental slip of the tool away from the targeted sample material. Two small holes 1cm and 2mm in size were drilled in the wax stage. The bigger hole was used to route a vacuum inlet into the block while smaller hole was used to hold the machinable sample under vacuum during machining so that excessive vibration and disturbance can be avoided which otherwise can create problems in machining. A simple pattern consisting of 8x3 holes was created using Dr. Engrave software. The gap between each hole was about 500µm. Each hole is represented as a single point on the software for the cut tool to make holes at these points with the hole size ranging accordingly with the cutting tool radius. Also a set of 5 lines was created each separated by 500µm distance. The lines were 1mm long and were of single point width on the software.

The CNC machine parameters, which affect the machining process, include the step depth of cut, linear cut speed in XY direction, which cuts in the plane of the sample, the vertical cut speed, or z-speed and the tool spin speed.[61] For the spin coated PMMA films, the single step depth was held at the minimum value of 10µm. The tool cut and spin speed were varied depending upon the pattern requirements. The range of cut spin speed was in terms of scale 1 to 15 where each represents 3000rpm and 8000rpm respectively. Approximately each unit represents a gain of about 335rpm.

For the process it was essential to detect the polymer surface to set a reference level for machining. The procedure to detect the surface was based on trial and error as several to and fro motion of the tool were made to visually detect any scratch produced while lowering and moving the tool slowly. The first vertical distance on the machine reading at which the scratch is seen is noted. A step back from this level is made vertically above the substrate and the position is fixed as zero reference level. If the machining does not produce any significant patterning the zero level is set a step below the initial zero and process is repeated.

4.3 Results and discussion

4.3.1 Spin coating

Spin coating of poly(methyl methacrylate) to form films of thickness greater than 10µm was desired for the machining experiments due to the minimum step depth reachable on the machine was only about 10µm. As an initial estimate, viscosity and spin coat data of SU-8 photoresist was taken for the spin coating experiments using PMMA. A 25µm thick SU-8 layer can be spin coated at a speed of 1000rpm from a solution of 1.5 Pa-s viscosity.[76] PMMA solution with an equivalent viscosity to that of the SU-8 was made using molecular weight, concentration and viscosity relationship.[77] Samples were made with approximately 20%, 30% and 35% by weight of PMMA solution in toluene, for solution viscosity equal to or greater than 1.5 Pa-s, and used for spin coating purposes. The viscosity of the solutions was calculated using available data.

Spin coating involves the effect of viscosity, solvent evaporation and spin speed.[78] The process tends to be difficult when resist thickness more than 10μm is desired[66] except in the case of special resists like SU-8 which can be made thick up to 200μm. Slow speeds or multiple coatings become necessary for greater thickness[66] but that can add to the non-uniformity of the film thus produced. The spin coating experiments are summarized in table-4.1. Samples were visually inspected for surface evenness. Low speed spin coating gave high uneven surface for the PMMA. For set-2, 1000rpm gave approximate thickness equivalent to 15μm. Spin coating of more than 2 coatings from set-1 gave non-uniform layers. From set-1 two layers spin coated at 1000rpm gave about 10-15μm thickness. The approximate thickness of the sample was estimated using profilometer by comparing the height difference between coated and non-coated surface of the sample. Spin coating of two layers at 1000 rpm resulted in non-uniform layering of films. Similar attempts on 35% PMMA gave non-uniform layers in all cases.

The basic criteria for a uniform spin coating of a film is sufficient centrifugal force to spread the solution since for insufficient force a non-uniform film layer is created.[66] Also the multiple spin coating might not add the individual thickness layer by layer as the spin speed and new top layer might also effect the original film thickness.[79] At low speeds the solution samples from set 1 with double coating and from set 2 were fairly planar (Table-4.1) and were used for machining experiments. Edge bead formation is generally seen for viscous solution spin coating[80] and was observed in most of the cases. The spin speed was controlled to obtain uniform spread on the surface by including acceleration steps to reach the desired spin speed level.[65] The acceleration was done manually by slowly tuning the speed control to the required speed. The acceleration was generally 20-50rpm per second. The solution was always flooded on the sample to ensure total coverage from spin coating.

Table:4.1. Summary of PMMA spin coating.

Sample Sets	**%PMMA in toluene**	**Spin speed** rpm	**Spin coated layer**	
			Layer 1	*Layer 2*
Set-1	20%	500	Smooth	Uneven surface
		1000	Smooth	Fairly even
Set-2	30%	500	Large beads at the edges, fairly smooth.	Uneven surface
		1000	Small beads at the edges, smooth surface	Not very planar surface
Set-3	35%	500	Uneven surface	Uneven surface
		1000	Uneven surface	Uneven surface

4.3.2 Holes: Cut spin speed and z-speed

Machining of holes was the simplest pattern that was attempted in these experiments. Generally PMMA is machined using parameters similar to copper at relatively low speeds.[62] The parameters normally associated with machining include the spin speed of the tool, the vertical speed of cut or z-speed, the continuous cut speed or linear speed in the plane of the sample (XY speed) and the depth of cut.[61] In the case of holes, the number of machining parameters reduce to two, tool spin speed and repeated machining. The other machining parameters held constant are depth of cut at 10µm, XY speed at 8 mm/second. The XY speed has no effect on the patterning of holes as no continuous machining is done on the plane of the substrate. The machining is done at the specified spin speeds and z-speed for the samples and the depth profile is estimated using confocal microscopy. In each case the machining resulted in non-smooth surfaces.

Sample from set 1 with 20% PMMA spin coated on glass coverslips, layer on layer, at 1000rpm was used to machine at a spin speed of 8000rpm. The layers were spin coated consecutively and the sample was heated at 150°C for 5 minutes on a hot plate. At this high temperature while the solvent is expected to evaporate the polymer also anneals at a temperature greater than the glass transition temperature of the polymer. Annealing is expected to hard bake the sample for better adhesion with the glass and also spread the polymer across the surface.[65] The sample when machined once using the available high speed of machining at 8000rpm and the z-speed fixed at 4mm/s, resulted in very rough surface profile. Figure 4.1 and 4.2 show that size of the hole is about 104µm while the depth of the cut is around 10µm. The machining creates a raised edge profile around the polymer as the tool displaces the material from inner regions (Figure 4.2). The bottom layer shows the crack marks from the tool in the material (Figure 4.1).

The extreme roughness in polymer film might be explained in terms of the glass transition temperature effects while machining a polymer. Generally smooth surface is obtained for surfaces when the polymer reaches the glass transition temperature while cutting.[62]

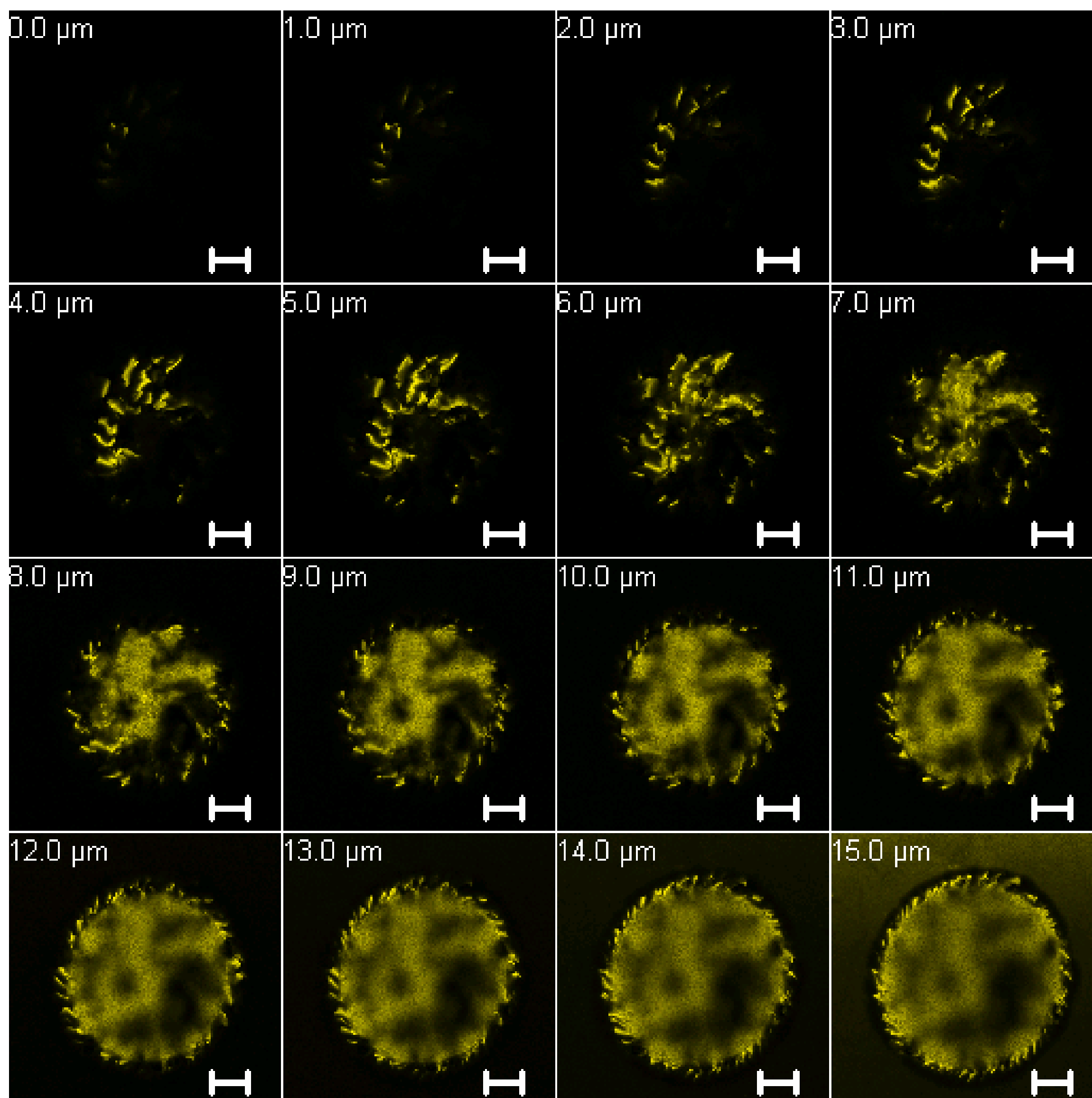

Scale bar 20 µm

Figure 4.1. CNC machined hole on PMMA. Left to right; top to bottom are the layered images of the machined hole in glycerol rohdamine and 1µm colloids. The cracks are visible at the bottom layer with a preferential clockwise direction, possibly the same sense of direction as the machining tool. Each layer is vertically 1µm apart. The number towards upper left side of the images is the relative distance between the layer in the image and the bottom most layer. The bar scale is 20µm and hole size is ~104µm

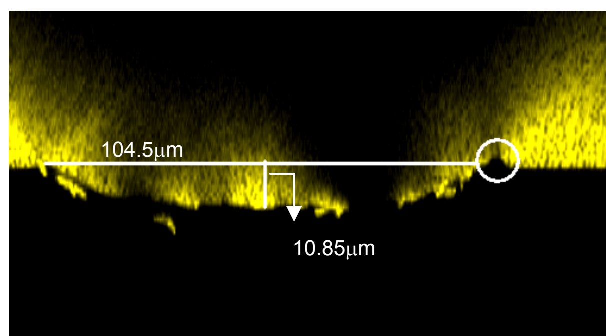

Figure 4.2. Side view of the CNC machined hole. The circle (right) shows the raised edges of the pattern.

Frictional heating tends to make the PMMA more ductile and more machinable. Under diamond machining conditions, PMMA behaves as ductile polymer as the frictional heating during diamond machining can reach the glass transition temperature for the polymer.[62] The roughness marks at the bottom show the material simply flowed along with the machining tool resulting in surface roughness. The excess softness of the polymer makes it unsuitable for machining purposes due to high liquid like response to machining, which makes the polymer simply flow along with the tool. With out any friction no heating takes place to shape the polymer while cutting. In this machining process, the depth of cut was safely around 10µm. The increase in hole dimension beyond 50µm could be attributed to possible shape divergence of the tool from the tip.

In the next approach sample from set 2 with 30% PMMA spin coated on the cover slip was heated at 50°C in the first step followed by heating at 150°C for 10 minutes. This two-step approach was used to reduce any bubble formation on the polymer surface and at the edge beads. This could be from the rapid solvent evaporation which might lead to the formation of bubbles at the edges. Machining was attempted at two different speeds while keeping the z-speed constant. Highest spin speed was used so as to reduce the surface roughness. The sample was machined at speeds of 3000 and 8000rpm. Figure 4.3 and 4.4 show no significant difference between the images and all the patterns have rough profile on the machined surface. One of the possible reasons for

the observed profile could be attributed to machining at a temperature less than the glass transition temperature of the substrate material. The maximum depth of cut was around 10µm in all the samples machined. The surface dimension of the hole was again more than 50µm. To obtain a smoother profile for the machined polymer, cutting speed greater than 8000rpm could be attempted.

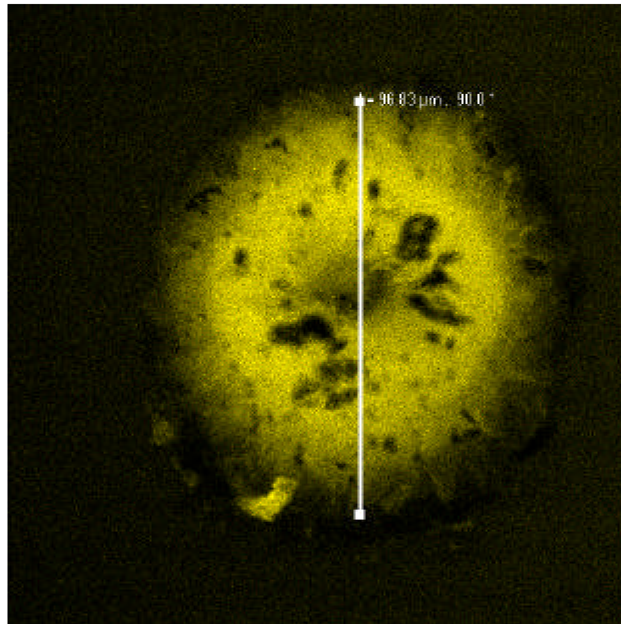

Figure 4.3. One time machined hole at a cut spin speed of 3000rpm. Dark regions show non-planar structures, which indicate roughness of the machined surface.

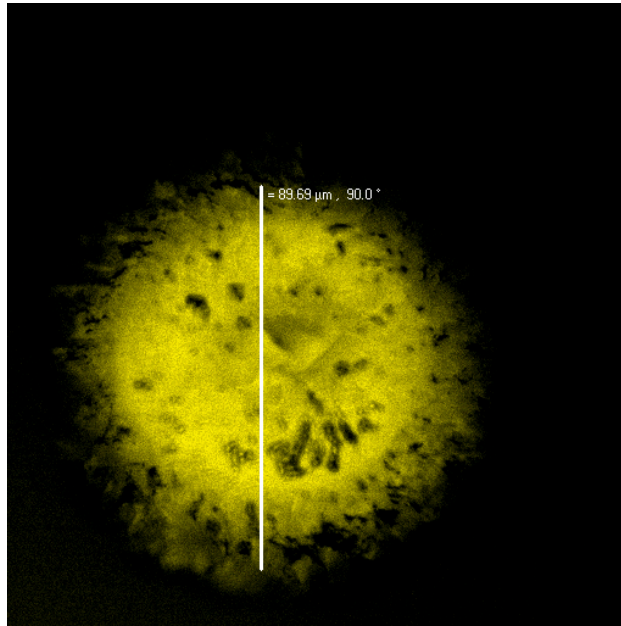

Figure 4.4. One time machined hole at a cut spin speed of 8000rpm. Dark regions show non-planar structures, which indicate roughness of the machined surface.

High z-speed while machining, results in stress in the polymer film leading to the formation of cracks.[61] Low z-speed machining becomes important in this case possibly along with high spin speed. Much lower speed might prove out to be useful for smooth profile machining for the spin coated pmma layers. The current available speed of 1mm/s is still high while machining a 10µm size pattern.

4.3.3 Number of repeats

The machining of the pattern was repeated in an attempt to reduce pattern roughness but did not result in any significant difference. Repeated machining can possibly improve the surface smoothness by reaching high temperatures for the sample. PMMA sample in figure 4.5 is a 30% solution from set 3; spin coated and baked at 50°C for 10 minutes and at 150°C for another 10 minutes. The machining removed material more from the sides as the raised part in the middle is seen in the dark regions of the figure 4.5 (b). Machining was done thrice at a speed of 5300rpm and z-speed fixed at

4mm/s. Three time machining resulted in rough surface as seen in the figure 4.5. Another sample was machined at 8000 rpm for the same z-speed and three repeats, still the roughness can be seen in the figure 4.6.

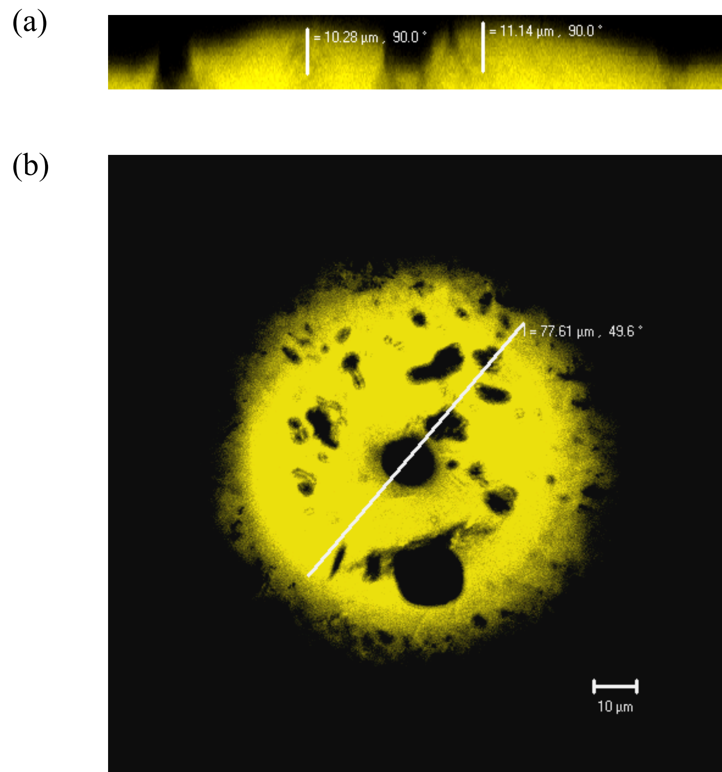

Figure 4.5. Hole machined repeatedly three times at 5300rpm. (a) Side view (upside down) of the pattern showing the raised region in the middle in dark. (b) Top view of the machined hole.

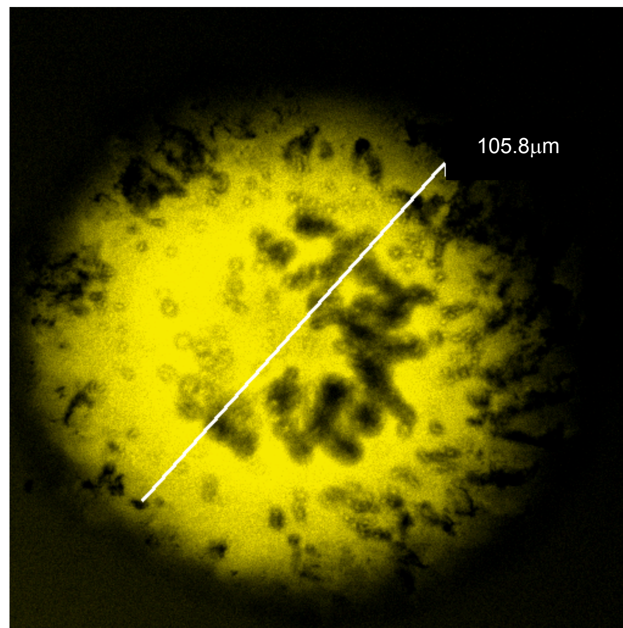

Figure 4.6. Hole machined at a speed of 8000rpm repeatedly three times.

Due to local surface unevenness, the cutting tool can machine through the sample to reach the glass surface. Figure 4.7 and 4.8 show the pattern machined through the film. The bottom part is flat due to glass surface while sidewall is machined polymer film.

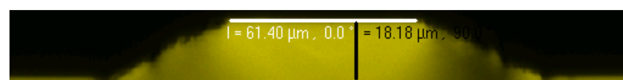

Figure 4.7. Cutting tool machined the PMMA to the glass surface: Side view. Image is upside down from confocal microscopy. Cut speed at 3000rpm and 3 times machining.

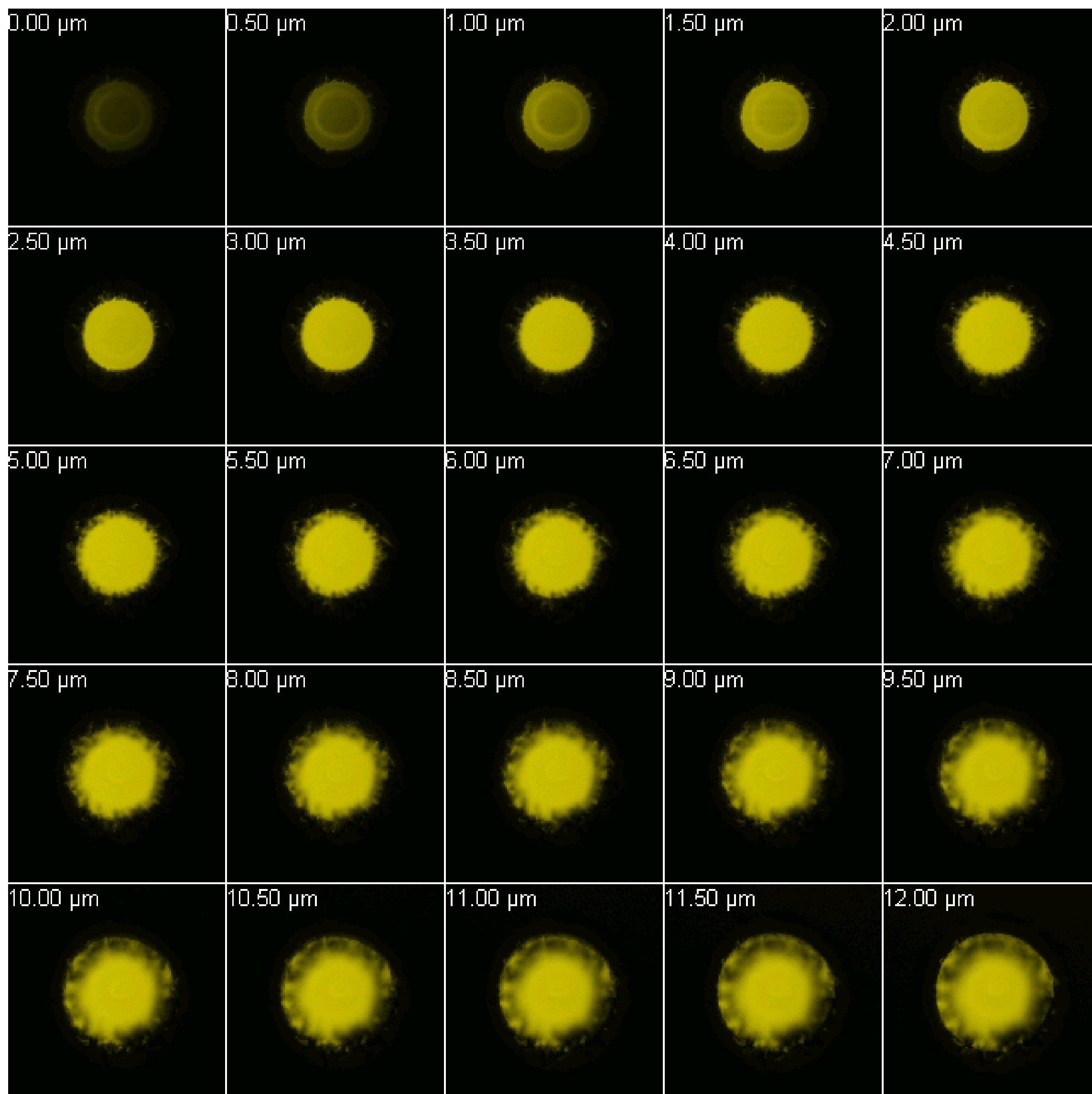

Figure 4.8. Cutting tool machined the PMMA to the glass surface: Layered top views. Image from left to right and top to bottom shows holes at various depths with an interval of 0.5μm. Cut speed at 3000rpm and 3 times machining.

4.3.4 Machining of lines:

The machining of lines involves two parameters the XY cut speed, which is the linear speed of the tool in the XY plane, and the spin speed. The maximum spin speed at 8000rpm was selected and kept constant. The XY speed was fixed at 8mm/s. The rough surface of machined lined in dark regions is shown in figure 4.9. As the figure 4.10 shows the wake of the tool as it machined the surface, the tool moves making continuous holes. The sample was pmma from set 3 heated at 150°C for 20 minutes.

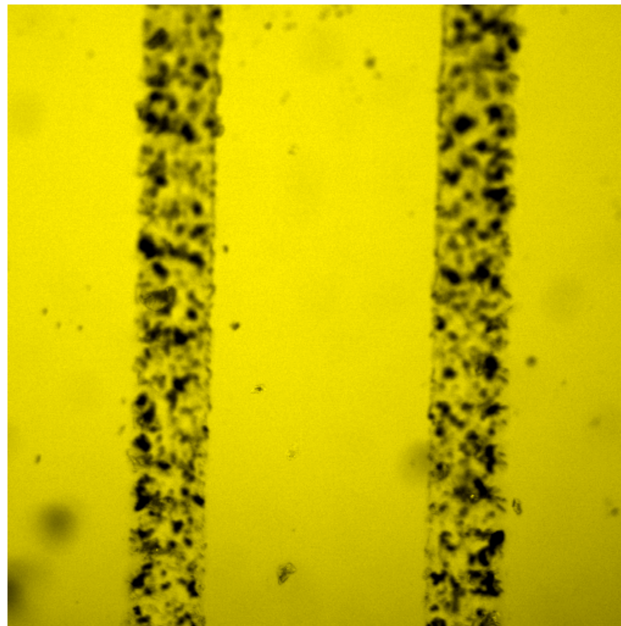

Figure 4.9. Line machined at a tool speed of 8000rpm. XY speed at 8 mm/s. The cracks are visible as dark regions.

Figure 4.10. Wake of tool (right) while machining line on PMMA. Image shows the machining of lines is continuously creating hole like structures. Local surface irregularity makes machining beyond the PMMA layer (left).

4.4 Conclusions

For PMMA solutions in toluene, high viscosity of solution resulted in uneven spin coating for solutions spin coated at same speed and duration. Also multi layer spin coating did not give very smooth surface. PMMA spin coating was attempted to give optimum layer thickness and smoothness at 30% concentration and 1000rpm for 40 seconds. The film resulted in beads at the edges and smooth surface at most of the spin coated surface.

The machining of spin coated polymer layer produced considerable roughness at all the tool cut speeds attempted. Also the unevenness of the polymer layer resulted in film breakage at certain places on the film as the fixed depth of cut exceeded the film thickness. A more uniform and precast thick polymer sheet can be used for machining to enhance the machinability of the polymer layers with a low ratio of depth of cut to the

thickness of the polymer film, to obtain better surface profiles of the patterns machined on the polymers. The machining of the polymer film at different cut speeds with specified z-speeds gave significant roughness in the surface profiles of the patterns. Holes of size range greater than known cut tool radius of curvature were seen while depth of cut ranged from 10 to 15μm. Also it can be assumed that glass transition temperature might not have been reached which resulted in non-smooth surface profile of the cut polymer. Much lower z-speed at high spin speeds can possibly result in better pattern features where the limiting factor for the size of the features was the size of the cutting tool involved.

5. OBERVATION OF PARTICLE PACKING ON TEMPLATE PATTERNS USING CONFOCAL MICROSCOPY

5.1 Introduction

This section involves the application of patterned templates from previous discussions in observing the packing of colloids in the template geometries. Particle arrangement was observed on relatively different pattern geometries using confocal microscopy. Confocal imaging of colloidal particles was made possible by the usage of optically transparent thin substrates, with particles in refractive index matched fluorescent solution. Particle packing, driven by gravity and capillary forces under the influence of physical pattern geometries, resulted in modest scattered order.

Colloidal crystallization using templates to direct the colloidal packing is known as colloidal epitaxy, which is a method similar to epitaxial growth of molecular crystals on defined single crystal planes of the substrates.[81] While using the same boundary conditions, i.e. the patterned templates, different forces and mechanisms that lead to particle and template interaction for colloidal crystallization include gravitational, entropic and capillary forces.

Capillary forces have been used to drive colloidal crystallization using flat as well as patterned templates. The capillary forces come into play due to the deformation of the liquid surface when the particles are partially immersed in a liquid film.[17] The capillary interaction between the particles increases with the interfacial deformation created by the particles.[82] The attractive forces between partially submerged particles lead to two and three-dimensional order. On a flat surface, the array formation for a colloidal particle suspension starts when the thickness of the water layer becomes equal to particle diameter and the crystal growth takes place through a directional motion of particles toward the ordered region.[17] Capillary forces and evaporating solvent thus induces colloidal crystals with controllable thickness on a flat micro slide. The limitation of colloidal crystallization on flat walls using these techniques is that the there

is less control on the symmetry and orientation of the crystal, which can be addressed by using patterned substrates.[83]

Capillary forces between particles and the influence of a patterned template via capillary forces on particle arrangement have been used extensively for colloidal crystallization. The 'V' shaped grooves etched into a silicon wafer provide a simple template for driving colloidal crystallization using capillary forces. The capillary forces and evaporation of dispersing agent drive the colloidal particles inside the groves and to close pack inside the grooves forming a pattern of ordered crystals.[18] Binary and ternary particle arrays can be fabricated by successive dip coating colloidal beads of different size onto the V shaped arrays of micro spheres.[27] In the template assisted self-assembly (TASA) method,[22] an aqueous dispersion of the colloids moves slowly across the bottom inclined surface until the particles are physically trapped inside the patterns. The colloidal beads within each template pattern close pack in the channels, in contact with each other and the wall due to the capillary forces and solvent evaporation.[22-24]

In this research, both glass and PMMA substrates were used for observing gravity and capillary force driven colloidal arrangement. Different pattern geometries and sizes along with fairly monodisperse polystyrene and silica particles were used for the purpose. The resulting arrangement along the substrate pattern geometries could be seen, though without any visible tendency towards large defined order. The influence of size mismatch between particle and pattern dimensions on the arrangement is also observed. Two to three particle layers were possible with in some of the pattern geometries. Subsequent packing, if any, tends to follow on these initially settled layers.[22]

For imaging, confocal laser scanning microscopy is used to obtain an in depth view of particle arrangement on the patterns with controlled precision through the bulk.[70] Confocal microscopy and a Fortran image-processing program were used together to image particles inside the patterns. Using both the techniques, particle packing can be observed in different view planes, which is useful in terms of obtaining a detailed and

independent description of particle arrangement in the confined geometries of the template patterns.

5.2 Experimental

5.2.1 Materials

Glass coverslips (corning 0211 zinc titania glass) were used as glass substrates. These are multi-component glass coverslips with SiO_2 64%, B_2O_3 9%, ZnO 7%, K_2O 7%, Na_2O 7%, TiO_2 3%, Al_2O_3 3%. Patterned PMMA layers spin coated on glass cover slips were used as polymeric templates. 20% and 30% PMMA (MW 120,000, Aldrich) solution was made in Toluene (Histornic grade, Aldrich). For confocal microscopy experiments, glycerol, dimethylformamide (DMF) or zeiss immersion oil was used as refractive index matching solution. Close refractive index matching reduces the amount of scattering for light when it passes through different media. Rhodamine (Fisher) was used for fluorescence in all of the solutions at 10^{-4}M concentrations. LSM 5 Pascal Zeiss confocal microscope was used for scanning the substrate and patterns. Polystyrene particles (duke scientific) of size 4μm or 6μm and 1μm Silica particles (polyscience) were used for colloidal deposition experiments.

5.2.2 Substrate preparation procedure

The glass substrate and PMMA was patterned following the procedure described in chapter 3 and chapter 4. Glass templates from wet etching generally have a profile with flat bottom and curved walls. Patterns etched using 1:10 buffered oxide etchant (NH_4F+HF) with 8μm depth and 20μm width at bottom surface were used to deposit colloids.

Isotropic etching in reactive ion etching method of glass coverslips created ellipsoidal profiles. The cover slips were etched in 14:2 standard cubic centimeter per minute (sccm) flow ratio of CF_4:O_2 at 200W for 60 minutes. The channels were 25μm wide on the surface with ~8-10μm depth.

Controlled 45 minute dry etching at 200W power, 10 sccm at 3:7 CF_4:O_2 flow rate and an intermittent 1M HCl wash to remove non-volatile products from the process, resulted in relatively straight wall trenches. The size of the patterns was approximately about 17μm in width and 6μm in depth.

PMMA patterns consisted of simple machined holes as described in chapter 4. The holes were machined at 3000 to 8000rpm with a maximum of three times repeated machining. The hole size on polymer substrates was as large as 100μm on the surface and a depth of ~12μm. The patterns were either completely in pmma or in some of the patterns the bottom layer was glass surface if the depth of cut exceeds pmma thickness.

5.2.3 Colloidal sample preparation

Particles of size 1μm, 4μm and 6μm diameter were used to prepare a solution in deionized water with a concentration capable to give approximately twice the monolayer coverage on the substrate. The glass substrates were cleaned in deionized water before depositing colloids on them. On the substrates, a 85μl colloid suspension was deposited and dried on the sample in open air without any disturbance. The substrates were placed perpendicular to gravity with no tilt.

It takes about 3-4 hours for the sample to get completely dry. On the dried sample, a single drop of refractive index matched solution with rhodamine is used. The sample is scanned using confocal microscopy. Similar procedure is repeated for PMMA substrate as well. For the glass substrates, the samples can be cleaned in deionized water with ultrasonication to remove the colloidal particles.

5.2.4 Confocal scanning laser microscopy

Confocal microscopy involves refining some of the imaging parameters for better scanning of the sample. The pinhole size was fixed at 100 for all the images. The pinhole blocks light from other parts of the sample while scanning a single spot repeatedly to create the image.[69] HeNe laser with 543nm wavelength was used at an excitation power level of 80. At this intensity the laser excites the rhodamine solution to

generate fluorescence while imaging the sample. The detector gain was varied around 500 numerical value and amplifier gain and offset were varied to obtain good image quality by adjusting the brightness and clarity of the image. A stack of images with specified X: Y: Z ratio (mostly at 1:1:1) is used to scan the images. The number of slices in the image stack was chosen so as to obtain complete depth of the view. 63X objective was used for imaging the particles. A zoom of 3 to 4 was used to obtain close-up images of the particles in the patterns.

For polystyrene particles in immersion oil solution, the scanning of sample is done with in 30 minutes as polystyrene particles begin to dissolve in the solution and imagining becomes difficult in this case. With silica particles, index-matching glycerol with rhodamine was also used to obtain fine images. Refractive index matching is important in order to reduce the scattering of laser light while traversing from different media. Fluorescence medium is used in order to obtain color-differentiated clear particle images.

5.2.5 Fortran image processing

The image stack from confocal is converted to tagged image file stack. For all the images for the code, the input image size of 512x512 pixels was used with a voxel ratio of 1:1:1 for X:Y:Z. Lateral side views and cross sectional views are generated along with the diagonal view using the program. Fortran code which converts the stack into three dimensional matrix produces side views of the plane along the image length. Modified code also creates image stack along the image width in a plane perpendicular to the stack and also along the diagonal of the stack (Figure 5.1). The code involves reading and writing manipulation of the image matrix. Along the diagonal view, the lateral dimensions are around 30% lower than the true value.

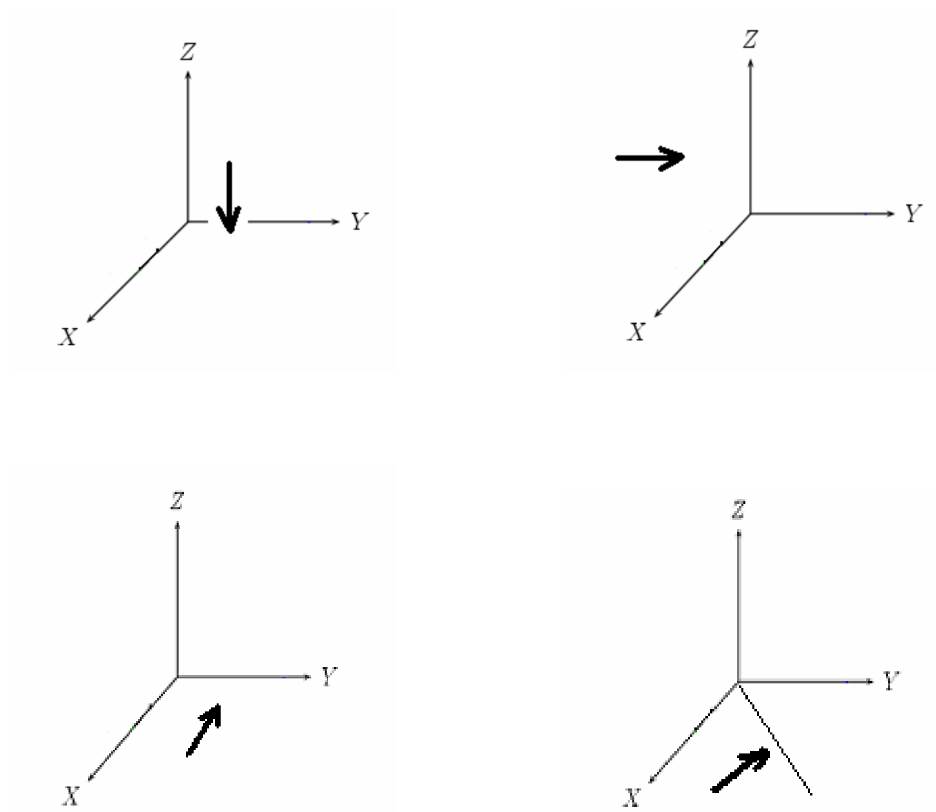

Figure 5.1. Fortran imaging: View planes. Images arranged clockwise from top: XY planes stacked along Z-axis, XZ planes stacked along Y-axis, ZY planes stacked along X-axis, and planes along the XY plane diagonal.

5.3 Results and discussion

5.3.1 Imaging of glass substrates*:*

Wet etching of glass substrates gives characteristic curved wall profile with a flat bottom as shown in figure 5.2. The pattern dimensions used in the following experiments were about 20µm at the flat bottom with approximately 5µm of depth. The latex particles used were 4µm in size. Particles were dried for about 3 hours and the dried sample was later scanned using fluorescent immersion oil.

In most of the channels the packing was greater towards the left, which might be due to the movement of the solution front as the sample solution dries on the surface. Long chains of colloids, along the trench edges towards left of the image, form probably as they accumulate along the trailing edge of a drying liquid layer (Figure 5.2). The evaporating liquid front tends to order the particle arrangement under the convective flow of particles.[18, 22, 83] The particles were able arrange themselves in a line at the flat bottom surface. The packing shows hexagonal order with line and point defects.

As mentioned earlier, capillary forces, which arise from drying solvent front, drives the colloids inside the groves and self-assembly is influenced by the drying process.[18, 22] Generally the particles assemble along the channel length[83] with subsequent

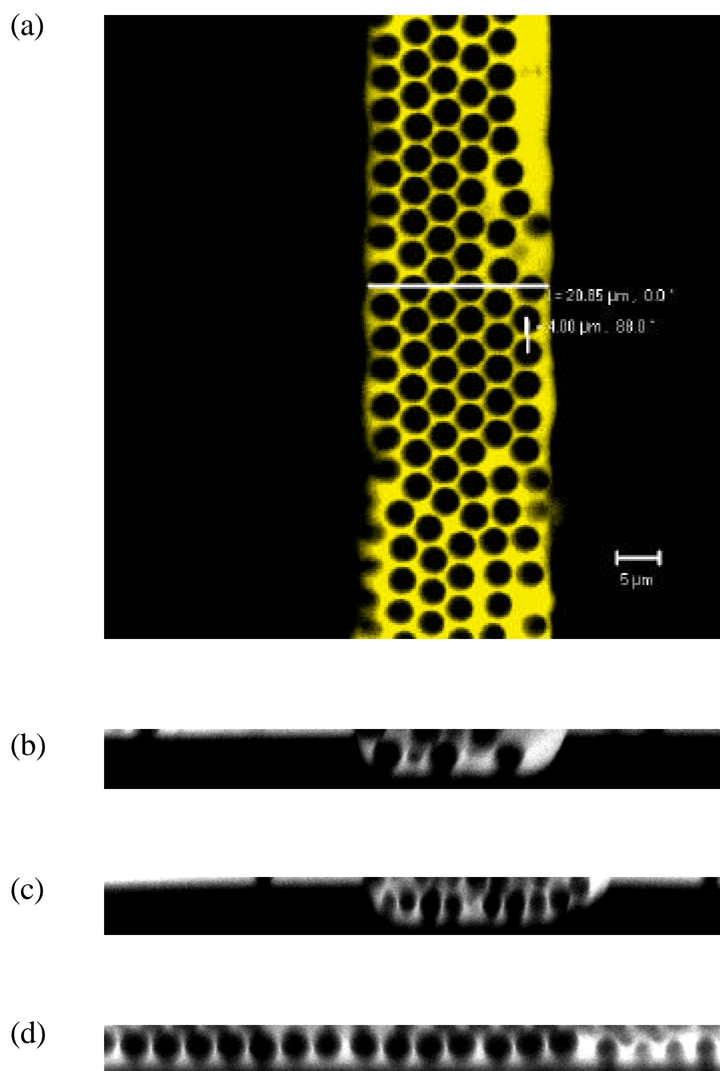

Figure 5.2. Colloids in channels patterned using glass wet etching. (a) Colloids self-assembled along the pattern edge towards left of the image. Layered 2D order is seen in the figure. The channels are flat bottomed and with curved wall. Lines from left to right close pack with line and point defects. (b) The particles formed straight lines along the channel edge. The side view shows long stretched chain of colloids. (c) Diagonal view of the particles in the channel. (d) The cross sectional view of the particles arranged in the channel.

next set of line, if any, forms adjacent to the first layer creating a two dimensional order. The particles have filled up a large section of the trench whereas lesser order can be seen at the lower end of the image. The side views show particles arrangement along the length with small distance of separation. Cross sectional view shows 3 particles in a plane.

Curved etch profiles on glass cover slips were made as the result of undercutting in reactive ion etch techniques. 4µm particles were used on the pattern, which was about 24µm wide on the surface and 8µm deep. In a curvilinear geometry no ordered arrangement was seen between particle layers (Figure 5.3). Particles occupied the channels less densely and random arrangement can be seen which can be attributed to increased instability in a curved geometry and lesser particle concentration. Unlike flat surfaces, the curved profiles tend to introduce additional defects and dislocations due to strain.[84] Few particles can be seen at the bottom of the trenches randomly distributed through out the pattern. Some order along the channel edges was seen. The arrangement of particles in channels depths was random with no visible order of arrangement of particles.

In relatively rectangular channels, made using the techniques discussed in chapter 3, were about ~8µm deep and 18µm-19µm wide on the surface with a nearly straight channel cross section. The particles tend to order at the bottom of the trenches. Particle arrangement along the edges was distorted probably due to the unevenness of the channel edges and local variation of the channel width added to the disorderly

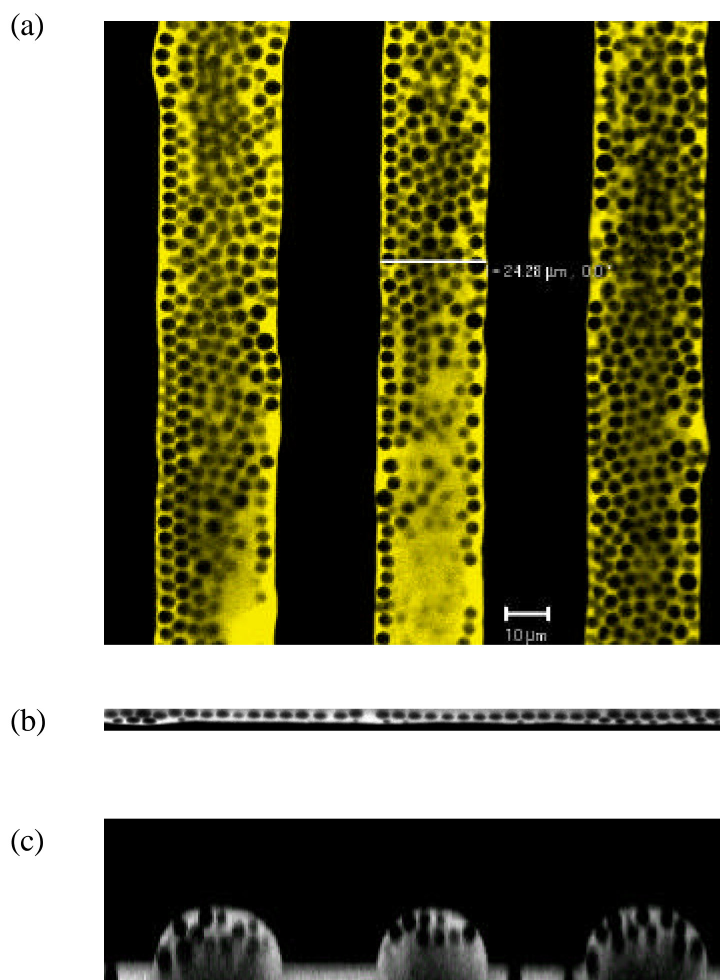

Figure 5.3. Colloids in curvilinear channels. (a) Ordered arrangement in the etched grooves is not seen in the case of curvilinear etch profiles. Particles formed long colloidal lines at some of the edges. The particle arrangement near one of the edges (channel towards left in (a)) shows that arrangement followed the edge profile closely. Channels are 14µm deep. (b) Side view of the partic les arranged along the edges. Long chain discontinues chain of colloids is seen in the image. (c) Cross sectional view of the particles arranged in the depth of the patterns (Image is up side down from confocal imaging).

arrangement. 4μm polystyrene particles were used for colloidal deposition on the template (Figure 5.4 and 5.5).

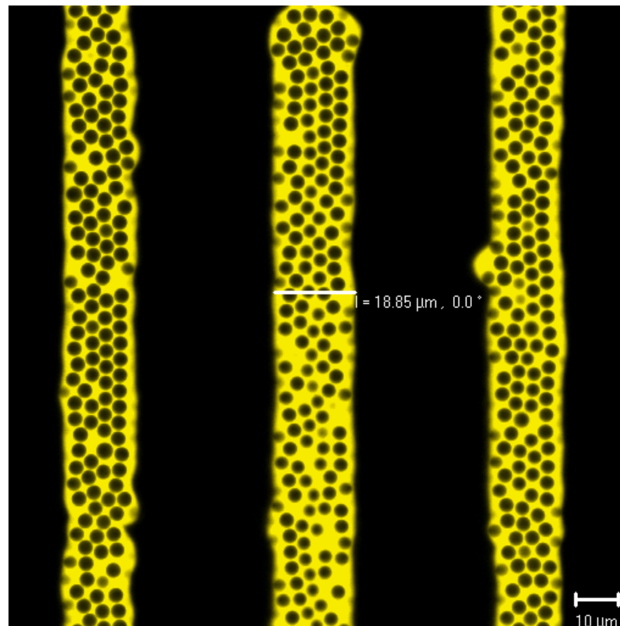

Figure 5.4. Colloids in pseudo-rectangular channels patterned using reactive ion etching. The unevenness and roughness of the edges created a very random arrangement of the particles. Particle arrangement along the channel edges was distorted by the edge profile. Some random ordering scattered on the pattern is seen in the image.

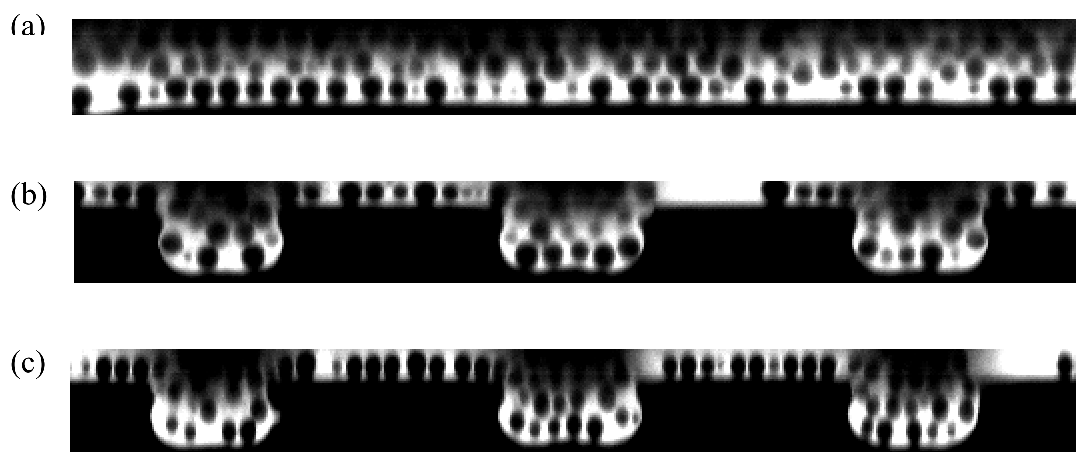

Figure 5.5. View planes of colloids in psuedo-rectangular channels. a) Side view: Particle packing in the channels along the edges did not show any formation of long chain of particles. The dark particles are in the plane of view and near the edge in the image. b) The cross section view of the particles inside the channels c) Diagonal view of the image stack show particles inside the channels. No order was seen in particle arrangement. Channels were 8μm deep.

5.3.2 Imaging of PMMA substrates

The PMMA template did not have smooth surface profile. The pattern consisted of ~100μm holes with around 10μm depth. Deposited particles arranged with in the confines of the patterns. The rough topography added disorder to the particle arrangement. 1 μm silica particles and 4 μm latex particles were used on the template. The capillary forces between the particle and pattern wall as well as between particle and particle generally tend to create an ordered particle arrangement.[25] Figure 5.6 shows 1μm particles in a 100μm hole. The relatively big pattern has no effect or clear influence on particle packing. The solution was not dried. Glycerol with rhodamine is used for scanning the image.

.

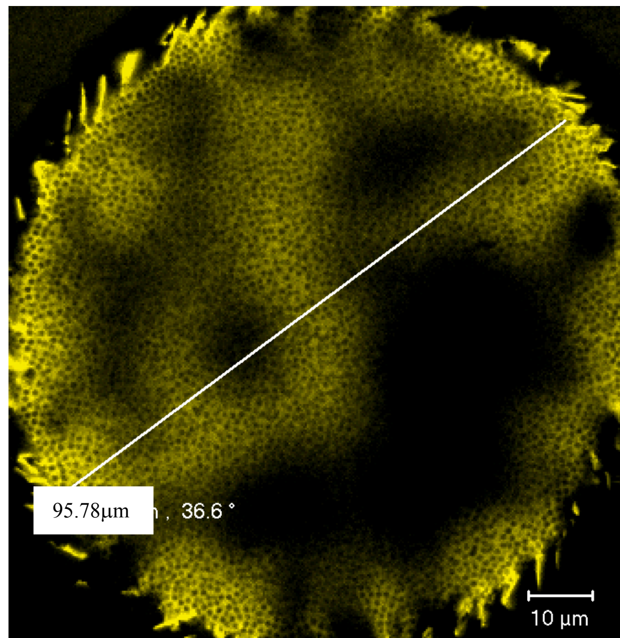

Figure 5.6. Silica particles confined in the rough geometries of the PMMA substrate. The diameter of the hole is about 96.78μm and depth about 12μm.

In figure 5.7 shows 4μm particles settled in a patterned hole. Side views show the particles settled around the raised middle section of the pattern. Rough and uneven profile again did not show any clear tendency of particles to pack in some order. Particles can be seen around the pattern edges and the central raised part of the pattern. Side views, cross sectional view and diagonal view images were not very clear probably due to refractive index mismatch between the particles, medium and template material.

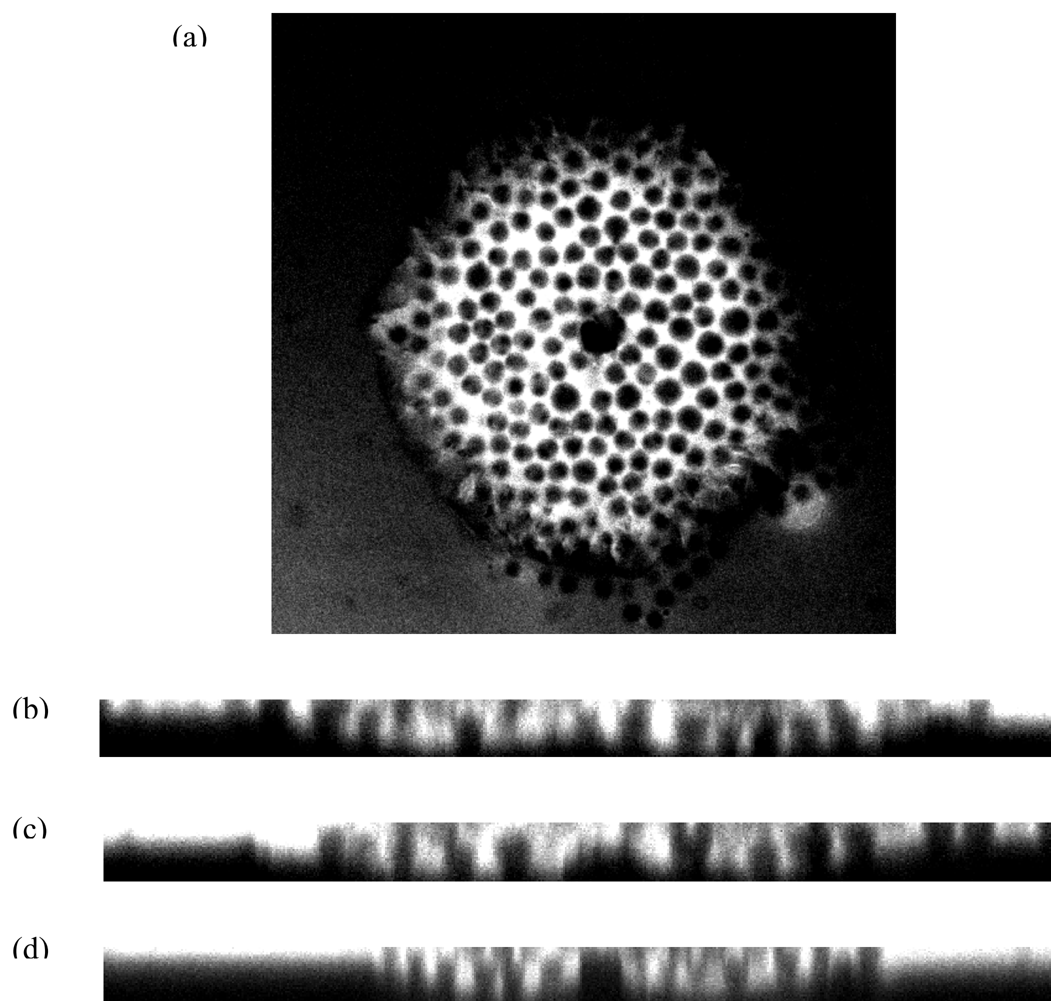

Figure 5.7. 6μm colloidal particles arranged in the machined PMMA hole. (a) The rough and uneven profile of the pattern created no order in the particle packing. Slight refractive index mismatch between PMMA, polystyrene particles and glycerol-rhodamine solution could have affected the quality of images. b) Side view of the particle arrangement in the pattern. c) Cross sectional view d) Diagonal view. Dark regions in the images are the particles while bright region correspond to the refractive index matched fluorescent medium. Hole size ~110μm in diameter and maximum depth of 12 μm.

In figure 5.8, the pattern is glass bottom with inclined PMMA walls. The machining through the pmma created this inclined profile. The polydispersity in the colloid sample can be seen. Few particles followed the inclined topography as shown in the figure 5.8(b).

(a)

(b)

(c)

(d)

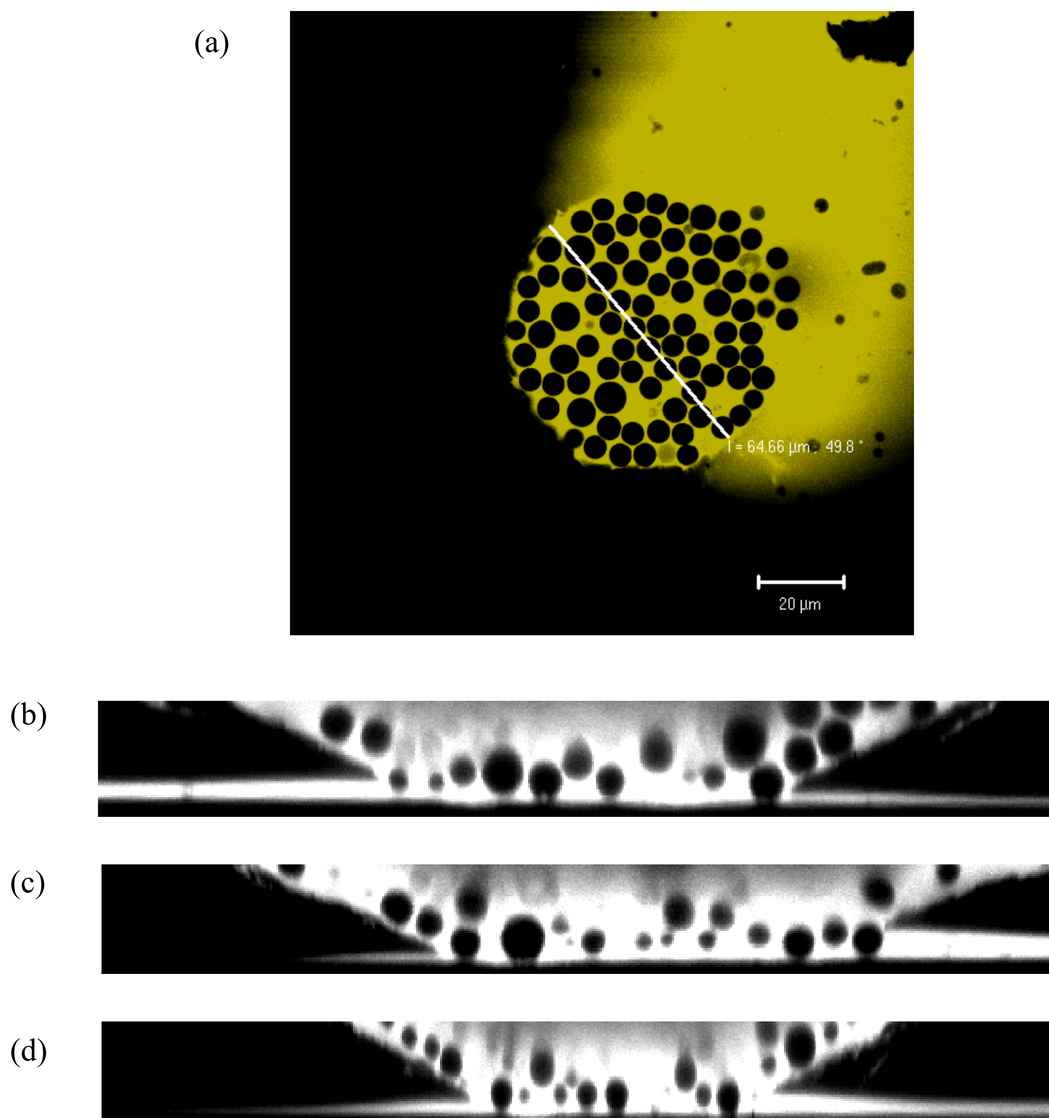

Figure 5.8. Polystyrene particles in the patterned hole with glass bottom and PMMA sidewalls. (a) The machining through the PMMA film created the above profile. As can be seen the particles also arranged along the inclined walls. Polydispersity in the sample is also shown in the above image. Depth of the machined hole is about 14µm. 6µm particles (polydisperse) were used on the sample. (b) Side view. (c) Diagonal view. (d) Cross sectional view.

No dense packing in the bottom is seen possibly due to low concentration of colloids used. Bright regions show the PMMA film was peeled from the glass surface. The fluorescent liquid entered beneath the PMMA on the glass surface.

5.4 Conclusions

Colloidal particles were deposited on patterned templates. Under the influence of gravity and capillary forces of drying, the particles were seen to assemble with in the confines of physical patterns. Glass and PMMA substrates were used as patterned templates with polystyrene or silica particles deposited on them. Confocal laser scanning microscopy and Fortran programming were used together to generate independent images of particle arrangements in the pattern geometries in 4 different view planes.

Curvilinear bottom profiles resulted in disordered arrangement where as some ordered arrangement and layering was visible in relatively straight flat bottom features. The influence of pattern is seen in the arrangement of the particles, as they tend to fit with in the pattern dimensions. Relatively low difference between the particle size and channel width as a factor of particle size resulted in more ordered arrangement.

The drying process tends to create the order from the walls. The 2D order tends to grow from the edges as seen in the glass substrate. Scattered order was seen in all of the patterned substrates. The arrangement also shows the tendency to follow the wall profile. Irregularities already present in the template and uncontrolled evaporation of the particle suspension resulted in less ordered packing of colloids.

6. CONCLUSIONS

6.1 Summary

In this research work, photolithographic and mechanical methods were used for fabricating patterns on glass and polymeric substrates. It was shown that reactive ion etching method on multi-component glass cover slips can be used to fabricate patterns with low undercut and fair degree of anisotropy compared to wet etching techniques. Computer numerical control (CNC) mechanical machining method was applied on spin coated poly(methyl methacrylate) (PMMA) films to create pre-specified patterns. These optically transparent and relatively thin templates were used for observing colloidal particle arrangement in confined pattern geometries.

Ultraviolet photolithography was used to transfer the patterns from a microfiche to the glass coverslips while including various micromachining processes. The pattern transfer was done using a positive photoresist after optimizing the exposure time for pattern transfer. For glass micromachining, both wet and dry etching methods were applied to create micrometer width channels with 4 μm to 10μm depth. Wet etching method using buffered oxide etching solution resulted in typical curved wall etch profiles with excessive undercut. Reactive ion etching method was attempted as a next step for patterning glass coverslips to limit the undercut during the patterning process. Multi-component glass etching in CF_4+O_2 plasma generally is made difficult due to the formation of non-volatile metal fluorides, which hinder and effect glass etching. Nickel was chosen as a suitable etch mask material after it resulted in reasonable etch profiles unlike the case with chrome and aluminum where etching was limited to or higher at the metal mask edges under similar etching conditions. In an attempt to control the isotropic etching of glass in dry etching, parameters like etch gas flow rate and flow ratios and power were varied. Etch rate increases with power and undercut increases with CF_4 ratio in the etch gas flow. Curved etch profiles were seen after the etch process, where undercut is seen to increase with the duration of etch. An intermittent 1M HCl wash was included in the process. This intermittent wash possibly removes the non-volatile

products from the etch surface and improves the process so as to create less undercut and produce relatively more anisotropic features on the coverslip glass. Nickel layer erosion was clearly seen at the edges on the coverslip after the etch process.

In the second method, computer numerical control machine (CNC) was used to pattern a spin coated thick poly(methyl methacrylate) film. Spin coating of PMMA to obtain a ~10μm or thicker film was attempted using spin coating multi-layers or high viscosity solutions. CNC machining is potentially a simple and fast method of polymer patterning using mechanical methods. Spin coating of 30% PMMA solutions at 20-50rpm accelerating spin speeds resulted in uniform surface coverage. Beads formed around the substrate edges due to high viscosity of the solution. PMMA machining was done with the available machining parameters and range. Machining at different tool spin speeds and repeated machining was attempted in order to optimize cutting conditions to get usable patterns. Pattern of holes was attempted where the size of hole on the surface was as large as 110μm, which can be possibly attributed to the shape and size of the tool. Machining at available high spin speeds and low feed rates or vertical tool speeds resulted in pattern profiles with considerable roughness.

In the final part of this research, the colloidal deposition on glass and polymeric templates was done using latex and silica particles. Polystyrene particles of size 4μm and 6μm were used on glass and PMMA template patterns. Silica particles of 1μm size were also deposited on to the templates. This process involves the self-assembly of particles under the influence of gravity and capillary forces of drying. Refractive index matched liquid, with rhodamine for fluorescence, was used to image the dried colloidal sample using confocal microscopy. Fortran program was used to process image slices at four different view planes to observe the particle arrangement in the pattern geometries. Image stacks of particles along the two lateral sides of the original confocal image stack and image stack along the diagonal plane of the image matrix are possible to observe the particle packing in the confined geometries of the templates Particles were seen to pack along the edges of the pattern features. No definite long-range tendency to form ordered structures was seen in the particles packed in the template pattern features. Particle

arrangement in curved pattern profile resulted in disordered arrangement along the pattern depth where as some order was seen for patterns with a relatively straight wall pattern profile.

7. FUTURE RESEARCH

7.1 Nanoindenting for patterning polymeric substrates

We have shown the results from the patterning of spin coated poly(methyl methacrylate) layers using computer numerical control (CNC) machining in earlier discussions. As stated earlier, down scaling of pattern features will depend on the size of the machining tool. Controlled machining to create further small features will require small machine tools. As an initial attempt nanoindentation of polymer templates was attempted to obtain feature size of patterns in ~1μm range.

Nanoindentation is also a mechanical process capable of creating micrometer range holes. It is basically used for measuring the strength of materials in terms of the force required to press a sharp diamond indenter into the target material to certain depth.[86] The basic parts of this equipment (Figure 7.1) are the indentor or tool, transducer and a piezoelectric material, which detect the surface and measure the force of application as specified.

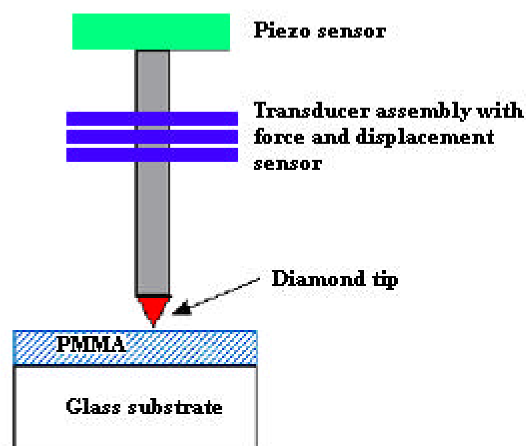

Figure 7.1. A nanoindentor basic set up.

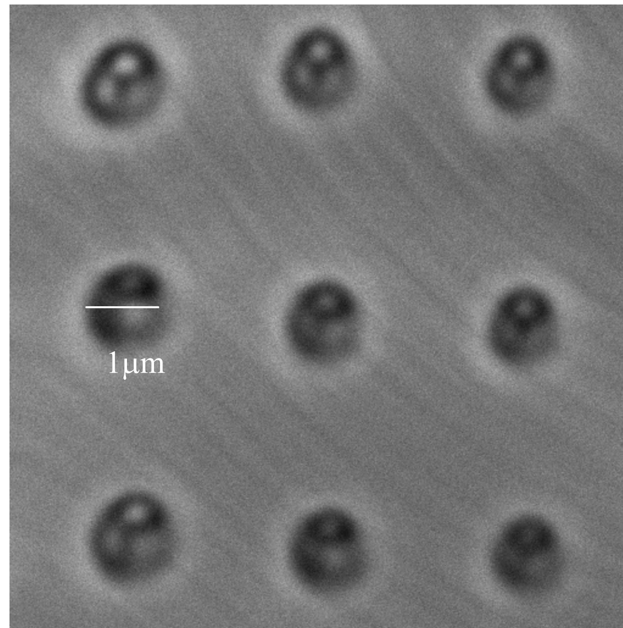

Figure 7.2. Simple hole pattern made using nanoindentor on a polymeric film.

In initial trials, patterns of one-micrometer size range were made using nanoindentor on a SU-8 polymer coated sample. This mechanical method was used to fabricate an array of holes of micrometer dimensions on the polymeric substrate. The negative photoresist SU-8 was spin coated on a glass substrate to obtain a ~5μm thickness. The substrate was attached to a metallic tip and placed inside the nanoindentor. The pattern was entered numerically and diagrammatically in the software while specifying the array of holes (Figure 7.2) as 10x10 set with distance between each hole kept at 3μm. The force of application was varied from 9000μm to 1000μm. Each column of holes was made using a constant force. A pyramidal shape diamond indenter was used for the purpose. The maximum force reached was about 8880μm, which resulted in a depth of 640nm. The lowest force of 282μN resulted in a depth of hole about 35nm in size. The width of holes in each case corresponds to the size of indenter.

Using this mechanical nanoindenting method, poly(methyl methacrylate) templates can be similarly fabricated when the size range of desired pattern is in ~1μm range. Unlike in e-beam lithography, this method does not require any metallic coating

on the polymer for pattern fabrication. These templates can be used for confocal microscopy experiments for studying the colloidal deposition on patterned polymeric templates. Also further work on computer numerical control (CNC) machining could be based on patterning of thin (~50μm) PMMA sheets attached to glass coverslips using cut tools with size ranges ~ 10μm or less fabricated using focused ion beam machining.[87] Increased speed can be attempted to possible give fine pattern surfaces.

7.2 Electrophoretic deposition of colloids on patterned templates

The patterned coverslips from this research work can also be used in studying electrophoretic deposition of colloids in confined template geometries. The external electric fields act to control the deposition rate of colloids.[87] Experiments related to template directed colloidal self-assembly require slow deposition of colloids on to the template where it is essential for the particles to have sufficient time to access low energy positions on the template and also form close pack structures with in sufficient time so as not to form glassy structures with random order.[6] Structures formed in micro gravity show that gravity effects the nucleation on growth of crystals by introducing stresses[88] so external control like electric field becomes necessary for controlled growth of colloidal crystals. Confocal microscopy studies of colloids in a controlled growth environment using electric fields and patterned templates will be useful to understand the effects of the confined geometries and electric field to direct the ordering process for charged colloids.

Indium tin oxide (ITO) is widely used as a conductive transparent material for electrophoretic experiments. The evaporation temperature of ITO is about 1800°C and a 10nm layer can be deposited on already patterned coverslips using physical vapor deposition techniques. Patterned cover slips which are now electrically conductive, thin and optically transparent can be used in confocal microscopy (Figure 7.3).

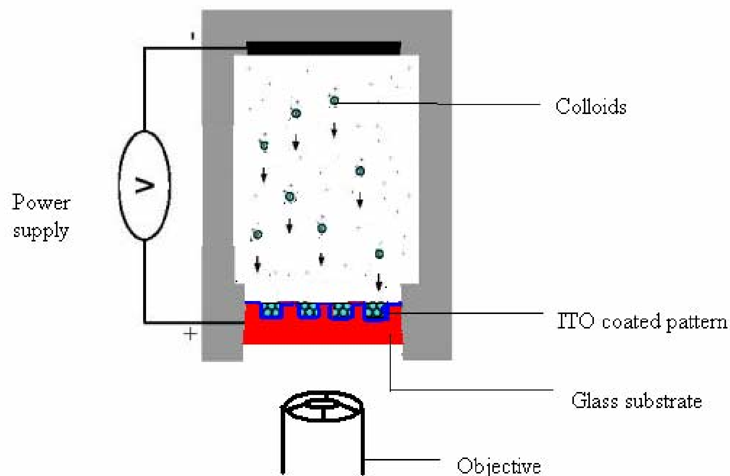

Figure 7.3. Electrophoretic deposition set up with ITO coated on patterned glass coverslips.

7.3 Quantitative assessment of Template directed colloidal crystallization

The reactive ion etching method described in this research can be further attempted to fabricate more precise and well-defined structures in 5μm or less size ranges on multi-component glass coverslips. Using a pattern defined on chrome photomask and the combined photolithography and etching techniques, microstructures with minimal undercut can be fabricated on thin glass coverslips. Fabrication of holes will be of particular interest since they can be used as potential energy wells for depositing colloidal particles. Particles deposited on to these templates can then be scanned using confocal microscopy. The images can be further processed using Fortran programming to generate independent images of particles packed in the template geometries. These images serve as a source to infer and asses the forces for attractive sphere system with an intention to understand its phase behavior.[89] Quantitative description of template directed colloidal crystallization in this case will be significant in the run up to control and manipulate the colloidal crystallization process.

7.4 Diffusing colloidal probe microscopy (DCPM)

The glass templates from this research can be used as masters for further template replication. Using soft lithography[89] the templates can be replicated to create reproducible polydimethyl siloxane (PDMS) stamps. These stamps can find their application in chemical patterning of substrates using microcontact printing. Physical glass templates, polymeric templates and chemically patterned templates can be used for DCPM related experiments for obtaining the potential energy profile of the patterned surface.[88] Using the mentioned information, site-specific colloidal deposition can be studied and monitored via confocal microscopy.

REFERENCES

1. Pieranski, P., *Contemporary Physics* **1983**, *24,* 25-73.

2. Sanders, J.V., *Acta Crystallogr.* **1968**, *A24,* 427.

3. Iler, R.K., *The Chemistry of Silica*; Wiley: New York, 1979.

4. Stober, W.; Fink, A.; Bohn, E., *Journal of Colloid and Interface Science* **1968**, *26,* 62-69.

5. Pusey, P.N.; Vanmegen, W.; Bartlett, P.; Ackerson, B.J.; Rarity, J.G., et al., *Physical Review Letters* **1989**, *63,* 2753-2756.

6. Davis, K.E.; Russel, W.B.; Glantschnig, W.J., *Science* **1989**, *245,* 507-510.

7. Sunkara, H.B.; Jethmalani, J.M.; Ford, W.T., *Chemistry of Materials* **1994**, *6,* 362-364.

8. Chang, S.Y.; Liu, L.; Asher, S.A., *Journal of the American Chemical Society* **1994**, *116,* 6739-6744.

9. Joannopoulos, J.D.; Villeneuve, P.R.; Fan, S., *Nature* **1997**, *386,* 143-149.

10. Tarhan, I.I.; Watson, G.H., *Physical Review Letters* **1996**, *76,* 315-318

11. Holtz, J.H.; Asher, S.A., *Nature* **1997**, *389,* 829-832.

12. Tirumkudulu, M.S.; Russel, W.B., *Langmuir* **2004**, *20,* 2947-2961.

13. van Blaaderen, A.; Ruel, R.; Wiltzius, P., *Nature* **1997**, *385,* 321-324.

14. van Blaaderen, A.; Wiltzius, P., *Advanced Materials* **1997**, *9,* 833.

15. Hoogenboom, J.P.; Yethiraj, A.; van Langen-Suurling, A.K.; Romijn, J.; van Blaaderen, A., *Physical Review Letters* **2002**, *89,* 256104.

16. Hoogenboom, J.P.; van Langen-Suurling, A.K.; Romijn, J.; van Blaaderen, A., *Physical Review Letters* **2003**, *90,* 138301.

17. Denkov, N.D.; Velev, O.D.; Kralchevsky, P.A.; Ivanov, I.B.; Yoshimura, H., et al., *Langmuir* **1992**, *8,* 3183-3190.

18. Yang, S.M.; Ozin, G.A., *Chemical Communications* **2000**, 2507-2508.

19. Ozin, G.A.; Yang, S.M., *Advanced Functional Materials* **2001**, *11,* 95-104.

20. Miguez, H.; Yang, S.M.; Ozin, G.A., *Langmuir* **2003**, *19,* 3479-3485.

21. Gates, B.; Yin, Y.D.; Xia, Y.N., *Chemistry of Materials* **1999**, *11,* 2827-2836.

22. Yin, Y.D.; Lu, Y.; Gates, B.; Xia, Y.N., *Journal of the American Chemical Society* **2001**, *123,* 8718-8729.

23. Yin, Y.D.; Xia, Y.N., *Advanced Materials* **2002**, *14,* 605-608.

24. Yin, Y.; Li, Z.Y.; Xia, Y., *Langmuir* **2003**, *19,* 622-631.

25. Xia, Y.N.; Yin, Y.D.; Lu, Y.; McLellan, J., *Advanced Functional Materials* **2003**, *13,* 907-918.

26. Jiang, P.; Bertone, J.F.; Hwang, K.S.; Colvin, V.L., *Chemistry of Materials* **1999**, *11,* 2132-2140.

27. Choi, D.G.; Yu, H.K.; Jang, S.G.; Yang, S.M., *Chemistry of Materials* **2003**, *15,* 4169.

28. Golding, R.K.; Lewis, P.C.; Kumacheva, E., *Langmuir* **2004**, *20,* 1414-1419.

29. Yodh, A.G.; Lin, K.H.; Crocker, J.C.; Dinsmore, A.D.; Verma, R., et al., *Philosophical Transactions of the Royal Society of London Series a-Mathematical Physical and Engineering Sciences* **2001**, *359,* 921-937.

30. Dinsmore, A.D.; Yodh, A.G.; Pine, D.J., *Physical Review E* **1995**, *52,* 4045-4057.

31. Dinsmore, A.D.; Yodh, A.G.; Pine, D.J., *Nature* **1996**, *383,* 239-242.

32. Zhang, J.; Alsayed, A.; Lin, K.H.; Sanyal, S.; Zhang, F., et al., *Applied Physics Letters* **2002**, *81,* 3176-3178.

33. Fudouzi, H.; Kobayashi, M.; Shinya, N., *Langmuir* **2002**, *18,* 7648-7652.

34. Braun, P.V.; Zehner, R.W.; White, C.A.; Weldon, M.K.; Kloc, C., et al., *Advanced Materials* **2001**, *13,* 721-724.

35. Lee, W.; Chan, A.; Bevan, M.A.; Lewis, J.A.; Braun, P.V., *Submitted to Langmuir* **2004**.

36. Yellen, B.B.; Friedman, G., *Langmuir* **2004**, *20,* 2553-2559.

37. Tien, J.; Terfort, A.; Whitesides, G.M., *Langmuir* **1997**, *13,* 5349-5355.

38. Friebel, S.; Aizenberg, J.; Abad, S.; Wiltzius, P., *Applied Physics Letters* **2000**, *77,* 2406-2408.

39. Korda, P.; Spalding, G.C.; Dufresne, E.R.; Grier, D.G., *Review of Scientific Instruments* **2002**, *73,* 1956-1957.

40. Cheng, Z.D.; Russell, W.B.; Chaikin, P.M., *Nature* **1999**, *401,* 893-895.

41. Holgado, M.; Garcia-Santamaria, F.; Blanco, A.; Ibisate, M.; Cintas, A., et al., *Langmuir* **1999**, *15,* 4701-4704.

42. Trau, M.; Saville, D.A.; Aksay, I.A., *Science* **1996**, *272,* 706-709.

43. van Blaaderen, A.; Hoogenboom, J.P.; Vossen, D.L.J.; Yethiraj, A.; van der Horst, A., et al., *Faraday Discussions* **2003**, *123,* 107-119.

44. Lin, K.H.; Crocker, J.C.; Prasad, V.; Schofield, A.; Weitz, D.A., et al., *Physical Review Letters* **2000**, *85,* 1770-1773.

45. Fan, Z.H.; Harrison, D.J., *Analytical Chemistry* **1994**, *66,* 177-184.

46. Corman, T.; Enoksson, P.; Stemme, G., *Journal of Micromechanics and Microengineering* **1998**, *8,* 84-87.

47. Bien, D.C.S.; Rainey, P.V.; Mitchell, S.J.N.; Gamble, H.S., *Journal of Micromechanics and Microengineering* **2003**, *13,* S34-S40.

48. Simpson, P.C., Woolley, A. T. and Mathies, R. A., *Biomedical Microdevices 1* **1998**, *1,* 7-25.

49. Roach, D.H.; Cooper, A.R., *Journal of the American Ceramic Society* **1986**, *69,* C153-C155.

50. Spierings, G.A.C.M., *Journal of Materials Science* **1993**, *28,* 6261-6273.

51. Stjernstrom, M.; Roeraade, J., *Journal of Micromechanics and Microengineering* **1998**, *8,* 33-38.

52. Lin, C.H.; Lee, G.B.; Lin, Y.H.; Chang, G.L., *Journal of Micromechanics and Microengineering* **2001**, *11,* 726-732.

53. Ronggui, S.; Righini, G.C., *Journal of Vacuum Science & Technology a-Vacuum Surfaces and Films* **1991**, *9,* 2709-2712.

54. Metwalli, E.; Pantano, C.G., *Nuclear Instruments & Methods in Physics Research Section B-Beam Interactions with Materials and Atoms* **2003**, *207,* 21-27.

55. Yue Kuo; J.R.C, *SPIE* **1988**, *945,* 103-110.

56. Zeze, D.A.; Forrest, R.D.; Carey, J.D.; Cox, D.C.; Robertson, I.D., et al., *Journal of Applied Physics* **2002**, *92,* 3624-3629.

57. Rodriguez, I.; Spicar-Mihalic, P.; Kuyper, C.L.; Fiorini, G.S.; Chiu, D.T., *Analytica Chimica Acta* **2003**, *496,* 205-215.

58. Leech, P.W., *Vacuum* **1999**, *55,* 191-196.

59. Li, X.H.; Abe, T.; Esashi, M., *Sensors and Actuators a-Physical* **2001**, *87,* 139-145.

60. Kobayashi, A.; Hirakawa, K., *Polymer-Plastics Technology and Engineering* **1984**, *22,* 15-25.

61. Kobayashi, A., *Machining of plastics*; McGraw-Hill: *USA,* **1967**.

62. Carr, J.W.; Feger, C., *Precision Engineering-Journal of the American Society for Precision Engineering* **1993**, *15,* 221-237.

63. Vasile, M.J.; Friedrich, C.R.; Kikkeri, B.; McElhannon, R., *Precision Engineering-Journal of the American Society for Precision Engineering* **1996**, *19,* 180-186.

64. Deng, T.; Tien, J.; Xu, B.; Whitesides, G.M., *Langmuir* **1999**, *15,* 6575-6581.

65. Campbell, S.A., *Science and Engineering of Microelectronic Applications*; Oxford University Press: New York, 1996.

66. Madou, M.J., *Fundamentals of Microfabrication: The Science of Miniarturization*; CRC Press: Boca Raton, FL, 2002.

67. Gandhi, S.K., *VLSI Fabrication Principles: Silicon and Gallium Arsenide*, 2nd Edition; John Wiley & Sons: New York, 1994.

68. Bazylenko, M.V.; Gross, M., *Journal of Vacuum Science & Technology a-Vacuum Surfaces and Films* **1996**, *14,* 2994-3003.

69. *LSM 5 Pascal, Laser Scanning Microscope*, Operating Manual, Carl Zeiss: Jena, Germany, 2002.

70. Dinsmore, A.D.; Weeks, E.R.; Prasad, V.; Levitt, A.C.; Weitz, D.A., *Applied Optics* **2001**, *40,* 4152-4159.

71. David S. Kiefer, M.I.A.D., Chandler, Arizona. Reactive ion etch recipes for failure analysis: Guiding note available at material characterization facility, (MCF), Texas A&M University, College Station, TX.

72. Yue Kuo; J.R.C., *SPIE* **1988**, *945,* 103.

73. Williams, K.R.; Muller, R.S., *Journal of Microelectromechanical Systems* **1996**, *5,* 256-269.

74. Nakata, H.; Nishioka, K.; Abe, H., *Journal of Vacuum Science & Technology* **1980**, *17,* 1351-1357.

75. Adams, D.P.; Vasile, M.J.; Benavides, G.; Campbell, A.N., *Precision Engineering-Journal of the International Societies for Precision Engineering and Nanotechnology* **2001**, *25,* 107-113.

76. Lorenz, H.; Despont, M.; Fahrni, N.; LaBianca, N.; Renaud, P., et al., *Journal of Micromechanics and Microengineering* **1997**, *7,* 121-124.

77. Dell'erba, R., *Journal of Materials Science Letters* **2001**, *20,* 371-373.

78. Gu, J.; Bullwinkel, M.D.; Campbell, G.A., *Polymer Engineering and Science* **1996**, *36,* 1019-1026.

79. S. Musa, N.L.; Sulur, G. Sengo; A. Driessen, *Proceedings symposium IEEE/LEOS Benelux Chapter, 2000 Delft, The Netherlands* **2000**.

80. Kelkar, P.S.; Beauvais, J.; Lavallee, E.; Drouin, D.; Cloutier, M., et al., *Journal of Vacuum Science & Technology A* **2004**, *22,* 743-746.

81. van Blaaderen, A.; Ruel, R.; Wiltzius, P., *Nature* **1997**, *385,* 321-324.

82. Kralchevsky, P.A.; Nagayama, K., *Langmuir* **1994**, *10,* 23-36.

83. Hoogenboom, J.P.; Retif, C.; de Bres, E.; de Boer, M.V.; van Langen-Suurling, A.K., et al., *Nano Letters* **2004**, *4,* 205-208.

84. Su, G.; Guo, Q.; Palmer, R.E., *Langmuir* **2003**, *19,* 9669-9671.

85. Bausch, A.R.; Bowick, M.J.; Cacciuto, A.; Dinsmore, A.D.; Hsu, M.F., et al., *Science* **2003**, *299,* 1716-1718.

86. Volinsky, A.A; Gerberich, W.W., *Microelectronic Engineering* **2003**, *69,* 519-527.

87. van Blaaderen, A.; Vrij, A., *Langmuir* **1992**, *8*, 2921.

88. Zhu, J.X.; Li, M.; Rogers, R.; Meyer, W.; Ottewill, R.H., et al., *Nature* **1997**, *387,* 883-885.

89. On going research in the Bevan research group, Chemical Engineering Department, Texas A&M University, College Station, TX.

90. Xia, Y.; Whitesides, G.M., *Angew. Chem. Int. Ed.* **1998**, *37,* 550-575.

VITA

Sumit Sharma graduated with a B.Tech. degree in chemical engineering from Jawaharlal Nehru Technological University, India in May 2002. In August 2002, he joined the Department of Chemical Engineering at Texas A&M University as a graduate student and received his M.S. degree in chemical engineering in December 2004.

Sumit Sharma may be contacted through Dr. Michael A. Bevan at the Chemical Engineering Department, Texas A&M University, College Station, Texas 77843.